# Tissue-specific Immunopathology in Fatal COVID-19

David A Dorward MBChB PhD[1,2], Clark D Russell MBChB[1,3], In Hwa Um PhD[4], Mustafa Elshani MSc[4], Stuart D Armstrong PhD[5], Rebekah Penrice-Randal MSc[5], Tracey Millar MSc[6], Chris EB Lerpiniere RGN[6], Giulia Tagliavini MSc[1],Catherine S Hartley MSc[5], Nadine P. Randle PhD[5], Naomi N Gachanja MSc[1], Philippe MD Potey MSc[1], Xiaofeng Dong PhD[5], Alison M Anderson MBE[7], Victoria L Campbell MBBS PhD[8], Alasdair J Duguid MB BChir[8], Wael Al Qsous MD[9], Ralph BouHaidar MD[2], J Kenneth Baillie MBChB PhD[10,11], Kevin Dhaliwal MBChB PhD[1,12], William A Wallace MBChB PhD[2], Christopher OC Bellamy MBChB PhD[1,2], Sandrine Prost PhD[1], Colin Smith MD[2,6], Julian A Hiscox PhD[5,13,14], David J Harrison MBChB PhD[2,4], Christopher D Lucas MBChB PhD*[1,12] on behalf of the ICECAP consortium.

[1]University of Edinburgh Centre for Inflammation Research, Queen's Medical Research Institute, Edinburgh BioQuarter, 47 Little France Crescent, Edinburgh, EH16 4TJ, U.K.

[2]Department of Pathology, Royal Infirmary of Edinburgh, 51 Little France Crescent, Edinburgh, EH16 4SA, U.K.

[3]Regional Infectious Diseases Unit, Western General Hospital, Crewe Road South, Edinburgh, EH4 2XU, U.K.

[4]School of Medicine, University of St Andrews, North Haugh, St Andrews, KY16 9TF, U.K.

AJRCCM Articles in Press. Published November 20, 2020 as 10.1164/rccm.202008-3265OC

[5]Institute of Infection, Veterinary and Ecological Sciences, University of Liverpool, ic2 Building, Liverpool, L3 5RF, U.K.

[6]Centre for Clinical Brain Sciences, University of Edinburgh, Chancellor's Building, Edinburgh BioQuarter ,49 Little France Crescent, Edinburgh, EH16 4SB, U.K.

[7]Mortuary Department, Royal Infirmary of Edinburgh, 51 Little France Crescent, Edinburgh, EH16 4SA, U.K.

[8]Department of Haematology, Western General Hospital, Crewe Road South, Edinburgh, EH4 2XU, U.K.

[9]Department of Pathology, Western General Hospital, Crewe Road South, Edinburgh, EH4 2XU, U.K.

[10]Roslin Institute, University of Edinburgh, Easter Bush Campus, Midlothian, EH25 9RG, U.K.

[11]Intensive Care Unit, Royal Infirmary Edinburgh, 51 Little France Crescent, Edinburgh, EH16 4SA, U.K.

[12]Department of Respiratory Medicine, Royal Infirmary of Edinburgh, 51 Little France Crescent, Edinburgh, EH16 4SA, U.K.

[13]Singapore Immunology Network, A*STAR, Singapore

[14]NIHR Health Protection Research Unit in Emerging and Zoonotic Infections, U.K.

AJRCCM Articles in Press. Published November 20, 2020 as 10.1164/rccm.202008-3265OC

ORCID ID: 0000-0002-4658-8829 (D.A.D.), 0000-0002-9873-8243 (C.D.R.), 0000-0002-2724-0325 (M.E.), 0000-0002-3862-1801 (S.A.), 0000-0002-0653-2097 (R.P-R.), 0000-0003-2210-9923 (G.T.), 0000-0001-9014-1015 (C.H.), 0000-0002-3775-9585 (N.P.R.), 0000-0002-5212-2574 (W.A.Q.), 0000-0001-5258-793X (J.K.B.), 0000-0002-3925-3174 (K.D.), 0000-0002-0140-7115 (S.P.), 0000-0002-4507-5132 (C.S.), 0000-0002-6582-0275 (J.A.H.), 0000-0001-9041-9988 (D.J.H.), 0000-0002-7523-0295 (C.D.L.).

*** Corresponding author:**

Christopher D. Lucas: christopher.lucas@ed.ac.uk

Tel: 0131 242 9100

University of Edinburgh Centre for Inflammation Research, Queen's Medical Research Institute, Edinburgh BioQuarter, 47 Little France Crescent, Edinburgh, EH16 4TJ.

**Author contributions:** DAD, CDL, CDR, JKB, DJH, JAH, CS: Conceptualization, Methodology, Validation, Formal analysis, Investigation, Data Curation, Writing – Original Draft, Writing – Review & Editing, Visualization, Supervision, Project administration, Funding acquisition. IHU, ME, SDA, RP-R, TM, CEBL, GT, CSH, NPR, VLC, AJD, WAQ, RB, COCB, SP, WAW: Investigation, Formal analysis, Writing – Review & Editing. KD, AMA, NNG: Resources. PMDP: Visualization.

**Sources of support:** ICECAP receives funding and support from The Chief Scientist Office (RARC-19 Funding Call, 'Inflammation in COVID-19: Exploration of Critical Aspects of Pathogenesis; COV/EDI/20/10' to D.A.D, C.D.L, C.D.R, J.K.B and D.J.H), LifeArc (through the University of Edinburgh STOPCOVID funding award, to K.D, D.A.D,

AJRCCM Articles in Press. Published November 20, 2020 as 10.1164/rccm.202008-3265OC

C.D.L), UKRI (COVID-19 Rapid Response Initiative; MR/V028790/1 to C.D.L, D.A.D and J.A.H) and Medical Research Scotland (CVG-1722-2020 to D.A.D, C.D.L, C.D.R, J.K.B and D.J.H). C.D.L is funded by a Wellcome Trust Clinical Career Development Fellowship (206566/Z/17/Z). J.K.B. and C.D.R. are supported by the Medical Research Council (grant MC_PC_19059) as part of the ISARIC Coronavirus Clinical Characterisation Consortium (ISARIC-4C). D.J.H, I.H.U and M.E are supported by iCAIRD (Industrial Centre for Artificial Intelligence Research in Digital Diagnostics). S.P. is supported by Kidney Research UK and Giulia by The Melville Trust for the Cure & Care of Cancer. Identification of SARS-CoV-2 and sequencing work was supported by the United States Food and Drug Administration grant number HHSF223201510104C 'Ebola Virus Disease: correlates of protection, determinants of outcome and clinical management' amended to incorporate urgent COVID-19 studies and contract number 75F40120C00085 'Characterization of severe coronavirus infection in humans and model systems for medical countermeasure development and evaluation' awarded to J.A.H. J.A.H. is also funded by the Centre of Excellence in Infectious Diseases Research (CEIDR) and the Alder Hey Charity. R.P.-R. is directly supported by the Medical Research Council Discovery Medicine North Doctoral Training Partnership. The group of J.A.H. is supported by the National Institute for Health Research Health Protection Research Unit (NIHR HPRU) in Emerging and Zoonotic Infections at University of Liverpool in partnership with Public Health England (PHE), in collaboration with Liverpool School of Tropical Medicine and the University of Oxford.

AJRCCM Articles in Press. Published November 20, 2020 as 10.1164/rccm.202008-3265OC

**Running title:** COVID-19 tissue immunopathology

**Descriptor:** 10.10 Pathogenic Mechanisms of Infections

**Word count:** 3202

This article has an online data supplement, which is accessible from this issue's table of content online at www.atsjournals.org.

Some of the results of these studies have been previously reported in the form of a preprint (medRxiv, [04 July 2020] https://doi.org/10.1101/2020.07.02.20145003).



AJRCCM Articles in Press. Published November 20, 2020 as 10.1164/rccm.202008-3265OC

## At a Glance

### What is the current scientific knowledge on this subject?

Inflammation is implicated in respiratory failure and death in severe COVID-19. The relationships between viral organotropism and organ-specific inflammatory responses have not been characterised, so it is unknown if inflammation is a direct response to the presence of SARS-CoV-2 or if virus-independent immunopathologic processes contribute.

### What does this study add to the field?

A disconnect between viral presence and inflammation implicates immunopathology as a primary mechanism of severe COVID-19. Specific immunopathologic features include mononuclear cell pulmonary artery vasculitis, pulmonary parenchymal expansion of monocytes/macrophages and stereotyped abnormal macrophage and plasma cell responses in the reticuloendothelial system, findings which validate ongoing investigations of immuno-modulatory and anti-inflammatory drugs in severe COVID-19.

AJRCCM Articles in Press. Published November 20, 2020 as 10.1164/rccm.202008-3265OC

## ABSTRACT

### Rationale

In life-threatening COVID-19, corticosteroids reduce mortality, suggesting that immune responses have a causal role in death. Whether this deleterious inflammation is primarily a direct reaction to the presence of SARS-CoV-2 or an independent immunopathologic process is unknown.

### Objectives

To determine SARS-CoV-2 organotropism and organ-specific inflammatory responses, and the relationships between viral presence, inflammation, and organ injury.

### Methods

Tissue was acquired from eleven detailed post-mortem examinations. SARS-CoV-2 organotropism was mapped by multiplex PCR and sequencing, with cellular resolution achieved by *in situ* viral spike protein detection. Histological evidence of inflammation was quantified from 37 anatomical sites, and the pulmonary immune response characterized by multiplex immunofluorescence.

### Measurements and Main Results

Multiple aberrant immune responses in fatal COVID-19 were found, principally involving the lung and reticuloendothelial system, and these were not clearly topologically associated with the virus. Inflammation and organ dysfunction did not


AJRCCM Articles in Press. Published November 20, 2020 as 10.1164/rccm.202008-3265OC

map to the tissue and cellular distribution of SARS-CoV-2 RNA and protein, both between and within tissues. An arteritis was identified in the lung, which was further characterised as a monocyte/myeloid-rich vasculitis, and occurred along with an influx of macrophage/monocyte-lineage cells into the pulmonary parenchyma. In addition, stereotyped abnormal reticulo-endothelial responses, including excessive reactive plasmacytosis and iron-laden macrophages, were present and dissociated from viral presence in lymphoid tissues.

**Conclusions**

Tissue-specific immunopathology occurs in COVID-19, implicating a significant component of immune-mediated, virus-independent immunopathology as a primary mechanism in severe disease. Our data highlight novel immunopathological mechanisms, and validate ongoing and future efforts to therapeutically target aberrant macrophage and plasma cell responses as well as promoting pathogen tolerance in COVID-19.

**Word count:** 259

AJRCCM Articles in Press. Published November 20, 2020 as 10.1164/rccm.202008-3265OC

## INTRODUCTION

Inflammation, organ injury and death due to viral infection can occur as a result of direct viral cytotoxicity, collateral damage from an appropriate pathogen-driven immune response, or an aberrant response precipitated by the pathogen, causing immunopathology (1). Resilience to infectious disease is frequently thought of as best achieved through resistance (controlling pathogen load to prevent organ injury) but the emerging concept of tolerance (preventing organ injury and inflammation despite the presence of pathogen) is equally valid (2). In this context tolerance could involve restricting the production of injurious inflammatory effectors or moderating pro- and anti-inflammatory signalling downstream of pathogen sensing, to reduce immunopathology (3, 4).

Hyper-inflammation is a recognised component of coronavirus disease 2019 (COVID-19), and associates with organ dysfunction, disease severity and death (5-7). Fatal COVID-19 most often occurs with critical impairment of oxygenation and treatment with corticosteroids has been robustly demonstrated to reduce mortality in these circumstances (8-13). This suggests that pulmonary inflammation has a causal role in death, but it remains unknown whether this inflammation is a direct response to the presence of SARS-CoV-2 or an independent immunopathologic process. Human immunology studies focusing on peripheral blood (7, 14) and bronchoalveolar lavage fluid (15) are revealing fundamental changes during COVID-19, but these approaches risk underestimating the immune changes within actual pulmonary tissue and so

AJRCCM Articles in Press. Published November 20, 2020 as 10.1164/rccm.202008-3265OC

immunophenotyping at a whole lung level in severe COVID-19 is essential. While COVID-19 is principally thought of as a pulmonary disease, increasing evidence shows that SARS-CoV-2 also has extra-pulmonary tissue tropism (16) and dysfunction of multiple organs occurs in COVID-19 (17). The relationship between presence of virus, evidence of organ injury and the associated immune response at a tissue and cellular level remains poorly defined.

In order to better understand the pathogen-host interaction and the immunological consequences of COVID-19, we present a multi-parameter tissue survey of fatal COVID-19. We sought to characterise and determine the relationships between viral organotropism and organ-specific immune responses. Some of the results of these studies were previously reported in the form of a preprint (18).

## METHODS

Detailed methods are available in the Supplementary Methods in the online data supplement.

### Post-mortem examinations

Post-mortem examinations were conducted in a biosafety level three (BSL3) post-mortem facility on patients with pre-mortem PCR-confirmed SARS-CoV-2 infection and evidence of lower respiratory tract disease at a median of 19·3 hours after death (interquartile range 4·6–20·2). 37 tissue sites were systematically sampled, following a standardised protocol, for histology and RNA analyses including 23 from the

AJRCCM Articles in Press. Published November 20, 2020 as 10.1164/rccm.202008-3265OC

respiratory tract (Figure E1). Samples were fixed in formalin or treated with TRIzol, snap frozen and stored at -80°C. Ethical approval was granted by the East of Scotland Research Ethics Service (16/ES/0084). Full clinical and radiologic details of our patient cohort are shown in Table 1, Figure E2 and Tables E1-2.

**Tissue histology and immunofluorescence**

Formalin-fixed paraffin-embedded (FFPE) tissue blocks were processed and haematoxylin & eosin stained following a standardised process in the hospital diagnostic pathology laboratory (19). Slides were reviewed by a group of specialist histopathologists who scored inflammation semi-quantitatively (none=0, mild=1, moderate=2, severe=3). For immunophenotyping, multiplexed immunofluorescence on de-paraffinised rehydrated FFPE slides was performed using combinations of primary antibodies against CD34, CD68, MRP8, CD4, CD8 and CD20, labelled with TSA-conjugated fluorophores, with antibody removal between steps. Images were captured using a Vectra Polaris slide scanner (Akoya Biociences). Control tissue for immunophenotyping was obtained from lung cancer resection specimens. Uninflamed lung tissue distinct from the site of carcinoma was utilised for immunofluorescence.

**Viral RNA and protein detection**

Total RNA was extracted at BSL3 from homogenised TRIzol treated tissue. Samples were DNAse treated and cDNA synthesised before amplification of SARS-CoV-2 by the ARTIC Network protocol using the multiplexed primer scheme version three. Purified

AJRCCM Articles in Press. Published November 20, 2020 as 10.1164/rccm.202008-3265OC

PCR products were processed, sequenced and analysed as per the appendix. Post-mortem interval was not associated with the number of tissue samples that were SARS-CoV-2 PCR positive post-mortem (Figure E3). De-paraffinised, rehydrated FFPE slides were examined for presence of SARS-CoV-2 spike (S) protein, with this performed on randomly selected SARS-CoV-2 PCR positive tissue from four patients, with or without additional cell markers (CD68 (mononuclear phagocytes), AE1/3 (epithelium) and CD105 (endothelium)), to detect viral presence**.**

## RESULTS

### Mapping SARS-CoV-2 distribution to tissue inflammation

To create a detailed tissue atlas of fatal COVID-19 we sampled 37 distinct anatomical tissue sites at autopsy to identify viral RNA distribution and host immune responses (Figure E1). We detected SARS-CoV-2 RNA across all sampled organs and tissue sites, most frequently in the respiratory tract but also from the gastrointestinal tract, heart and muscle, and less often from the liver, kidney and other organs (Figure 1 A,B). Despite all sampled organs having the potential to contain SARS-CoV-2 RNA, we observed substantial inter-patient variation in the tissue sites involved (Figure 1B). The time from illness onset to death did not correlate with the number of PCR-positive organs (Figure 1B; Figure E3). Results from multiplex PCR were confirmed to map to the SARS-CoV-2 genome by sequencing (Figure 1 C,D) significantly increasing confidence in these data compared with a PCR-only approach. Viral subgenomic

AJRCCM Articles in Press. Published November 20, 2020 as 10.1164/rccm.202008-3265OC

messenger RNA (most commonly from the nucleocapsid gene) was also detected from PCR-positive sites, indicating active viral RNA synthesis had occurred (Figure E4).

As analysis of SARS-CoV-2 RNA confirmed presence in numerous organs, detailed tissue analysis was undertaken on every patient to determine the associated pathological consequences and immune responses. In contrast to the distribution of viral RNA, this analysis indicated that the lung and reticulo-endothelial system were the exclusive sites of an extensive inflammatory response (Figure 1A). Extra-pulmonary sites with virus present, and evidence of viral transcription, did not have substantial local inflammation.

To better resolve this organ-specific pathogen-host interaction at a spatial and cellular level, the presence of SARS-CoV-2 S protein was evaluated on randomly selected SARS-CoV-2 PCR-positive tissues. Consistent with the latest reports on tissue expression of SARS-CoV-2 entry factors (20), S protein was found predominantly within epithelia of the aero-respiratory tract, gastrointestinal tract, liver and kidney, with limited presence within macrophages ($CD68^+$ cells) and endothelial cells ($CD105^+$ cells) of lung tissue (Figure 1 E-F). The S protein was only rarely detected in some of the SARS-CoV-2 PCR negative tissues tested, and not in post-mortem tissues from patients who did not have SARS-CoV-2 infection (data not shown). While SARS-CoV-2 S protein expression within lung alveolar epithelial cells was patchy in nature, consistent with possible aspiration or inhalation of virus from the upper respiratory tract (21), expression at non-pulmonary sites frequently revealed several well demarcated areas

AJRCCM Articles in Press. Published November 20, 2020 as 10.1164/rccm.202008-3265OC

of confluent SARS-CoV-2 S protein expression within adjacent cells, surrounded by cells with no detectable protein (Figure 1 E). These 'foci of infection', with numerous affected cells adjacent to unaffected cells, are suggestive of cell-to-cell spread as reported in other coronavirus and respiratory viruses (22, 23).

Overall, we observed minimal evidence of acute inflammation in other organs (Figure 1 A). Background changes of chronic disease were common, reflecting pre-existing co-morbidities. Expected organ injury commensurate with severity of systemic illness was also present (e.g. renal acute tubular necrosis in mechanically ventilated patients, Table E3). Detectable viral RNA in the kidney (n=4 detectable), liver (n=4) and gastrointestinal tract (n=7) was not associated with inflammation scores or with biochemical evidence of acute kidney injury, peak ALT measurement or enteric symptoms, respectively (Figure E5). No acute tissue abnormalities were identified in the gastrointestinal tract or endocrine organs and no cases of myocarditis were identified despite frequent detection of viral RNA within these tissues (Table E3). Importantly, the presence of viral protein within the kidney (n=4 assessed), intestine (n=3) and liver (n=2) were not associated with a localised inflammatory response adjacent to the infected cells (Figure 1 E-F; Figure E6).

**Pulmonary inflammation and relationship to SARS-CoV-2**

Pulmonary tissue was highly abnormal, with diffuse alveolar damage (DAD, the pathological hallmark of Acute Respiratory Distress Syndrome; ARDS), thrombosis and bronchopneumonia frequent but variable findings (Figure 2A). Unexpectedly, the

AJRCCM Articles in Press. Published November 20, 2020 as 10.1164/rccm.202008-3265OC

geographical distribution of SARS-CoV-2 RNA presence within the lung was not linearly associated with pulmonary inflammatory changes within our cohort as DAD and bronchopneumonia were both observed in sections of lung with and without detectable virus. In one patient (Patient I) virus could be detected in the absence of significant pulmonary inflammation. These findings strongly suggest that virus-independent immunopathology, rather than direct viral cytotoxicity, is one of the primary mechanisms underlying severe COVID-19.

Consistent with recent reports, pulmonary thrombi were present in multiple patients (8/11; small vessel only n=1, large vessel only n=2, large and small vessel n=5) (Figure 2A). A patchy but striking mononuclear cell vasculitis predominantly affecting intima of small/medium sized pulmonary arteries was also observed in 4/11 cases (Figure 2B). This pulmonary artery immune infiltrate was further characterised in two patients (A&C) by multiplex immunofluorescence (Figure 2 C,D). Unexpectedly, $MRP8^+$ mononuclear cells were the predominant infiltrating population accompanied by a mixed population of $CD4^+$ and $CD8^+$ T cells and macrophages (Figure 2 C,D). Inspection of 40 inflamed vessels from the same patients did not identify SARS-CoV-2 S protein within the surface endothelium (data not shown). No vasculitis was evident in any of the other organs studied.

Increased $CD8^+$ T cells and reduced resident lung macrophages have recently been reported using single cell transcriptomics on bronchoalveolar lavage fluid (BALF) cells (15). However, this approach risks underestimating pathophysiological and immune

AJRCCM Articles in Press. Published November 20, 2020 as 10.1164/rccm.202008-3265OC

changes within the non-luminal pulmonary compartment. To understand the immune response at a whole lung level multiplex immunophenotyping was undertaken on pulmonary tissue (Figure 3 A-G; Figure E7). Our analysis revealed that the greatest increase in immune cells were predominantly within parenchymal regions rather than vascular/perivascular areas (Figure 3F-G). This showed that the largest relative increases were within the mononuclear phagocyte compartment ($CD68^+/MRP8^-$ macrophages, then $CD68^+/MRP8^+$ monocytic cells) followed by $CD8^+$ then $CD4^+$ T cells. Smaller increases in $CD20^+$ cells and $MRP8^+/CD68^-$ cells were also observed.

**Reticulo-endothelial system responses in fatal COVID-19**

All cases showed a severe and stereotyped pattern of immunological changes regardless of viral RNA presence within the lymph node or spleen (Figure 3 H-J). Within the bone marrow, erythroid dysplasia, plasma cell excess with morphological atypia and iron storage abnormalities were identified (Figure 3H,I, Figure E8, Table E4). A marked increase in the number of plasma cells (5% or more) was seen in 5/8 bone marrow aspirates but these plasma cells had a normal phenotype on bone marrow trephines, being negative for CD56 and cyclin D1, and were polytypic with light chain immunohistochemistry (Figure E8). Iron laden macrophages were seen in all but one case examined (7/8) and associated with abundant iron storage on Perl's stain. Although infrequent (1-2/1,000 cells), haemophagocytosis of erythroid and/or myeloid precursors was present in bone marrow in three cases. In mediastinal lymph nodes, marked reactive plasmacytosis of $CD38^+/MUM1^+$ and weakly CD138+ cells were seen

AJRCCM Articles in Press. Published November 20, 2020 as 10.1164/rccm.202008-3265OC

in the paracortex and medulla, again exhibiting a degree of nuclear pleomorphism. In the spleen, white pulp atrophy was common (4/7) similar to post-mortem observations in fatal SARS (24, 25). Splenic red pulp was congested and, in all cases, contained an increased number of plasma cells with similar features to those observed in mediastinal nodes.

## DISCUSSION

The data presented in this manuscript have several implications for our understanding of severe COVID-19. Firstly, we show that fatal COVID-19 is associated with variable but widespread distribution of viral RNA and protein but with an unexpected discordant inflammatory response to local viral presence, both between and within tissues. If organ injury is primarily collateral damage to an appropriate local inflammatory response against SARS-CoV-2, it would be expected to have a temporal and spatial association with the presence of the virus. We have observed the opposite. In some cases inflammation was present in sections of lung without detectable virus (and in patients who had not received invasive mechanical ventilation). This could relate to non-resolving inflammation after viral clearance, or inflammation in areas of lung where viral replication had never occurred; considering the sensitivity of PCR for viral detection, we contend the latter is possible. Conversely, even at the time of death, up to 42 days after illness onset, viral products (both RNA and protein) and evidence of viral RNA synthesis (subgenomic mRNA) could be detected in numerous tissues but dissociated from host inflammatory responses. Furthermore, the time from illness

AJRCCM Articles in Press. Published November 20, 2020 as 10.1164/rccm.202008-3265OC

onset to death did not correlate with the number of PCR-positive organs. The presence of viral RNA within the kidney, intestine and liver was not associated with evidence of organ injury or inflammation. By spatially resolving viral presence we confirmed that in extra-pulmonary tissues, cells containing the SARS-CoV-2 S protein did not have an adjacent localised cellular immune response. These findings are consistent with strains of avian coronavirus which can replicate in the gut without causing macroscopic or histological changes (26). While lung tissue was frequently highly abnormal, to our surprise the geographical distribution of SARS-CoV-2 RNA presence within the lung was not linearly associated with either the presence or nature of the lung inflammatory response. Within our cohort, we report both DAD and bronchopneumonia in sections of lung with and without detectable virus, as well as viral presence but without inflammation. Together, these observations on the immunopathology in relation to SARS-CoV-2 reveal an aberrant immune response, principally involving the lung and reticuloendothelial system, that is not clearly topologically associated with viral presence. This is clinically relevant: the evidence we present of virus-independent immunopathology being a primary mechanism underlying fatal COVID-19 supports the prioritisation of tolerance as a therapeutic strategy. This is consistent with the beneficial effect of corticosteroids in severe disease (13) and importantly provides a potential biological mechanistic basis for their efficacy, validating ongoing investigations of immuno-modulatory and anti-inflammatory drugs (27).

AJRCCM Articles in Press. Published November 20, 2020 as 10.1164/rccm.202008-3265OC

Secondly, we expand upon the observation of increased $CD8^+$ T cells and reduced resident lung macrophages in BALF(15), by describing a marked relative increase in immune cells of the mononuclear phagocyte lineage, and to a lesser extent $CD4^+$ and $CD8^+$ T cells, within the non-luminal pulmonary compartment. Macrophage abnormalities were also seen within bone marrow, with iron laden macrophages observed in all but one patient, despite the absence of typical causes of secondary iron overload (transfusion, haemolysis), and is consistent with the observation that circulating ferritin correlates with adverse outcomes(28). In human immunodeficiency virus and hepatitis C virus infection, iron overload is associated with poor prognosis, with evidence that viral infection itself may enhance macrophage iron loading, further suggesting that iron overload is an aberrant macrophage response deleterious to the host in COVID-19(29).

Third, consistent with emerging literature, small and large pulmonary vessel thrombi were common in our series (30-32). Thrombi in pulmonary vessels have also been reported in fatal cases of SARS (24, 33), influenza A virus infection (34, 35), and ARDS more generally, but the frequency in COVID-19 appears nearly a log order higher compared to influenza and may be due to distinct endothelial injury pathways(30) but the drivers of this are unknown. Here we describe an immune cell pulmonary arteritis in nearly half of our cases, a novel pathological process in severe COVID-19 that may contribute to endothelial cell dysfunction and vascular thrombosis, and could represent a therapeutic target. Phenotyping of this pulmonary vasculitis revealed that

AJRCCM Articles in Press. Published November 20, 2020 as 10.1164/rccm.202008-3265OC

the primary immune cells are not infiltrating T cells, in contrast to reports in fatal influenza (30), but MRP8$^{+}$ mononuclear cells infiltrating into vessel walls. This COVID-19 vasculitis was not associated with local endothelial viral S protein expression although S protein was identified within a small number of CD105$^{+}$ endothelial cells in other vessels within the lung. This observation validates the drive to understand the immune microenvironment at a whole lung level and is particularly interesting considering the identification of pro-inflammatory monocyte-derived macrophages in bronchoalveolar lavage fluid (15) and the recent report of C5aR1$^{+}$ macrophages associated with obliterating arteritis in a COVID-19 autopsy sample, implicating mononuclear phagocyte activation and expansion as important pathologic processes in COVID-19 (36). Indeed, therapeutic targeting of the C5a axis has been proposed (37). The observation is also consistent with the finding that the myeloid growth factor GM-CSF and the monocyte/macrophage chemoattractant MCP-1 are elevated in blood and associated with COVID-19 severity(38, 39). Going forward, it will be important to clarify whether these macrophage abnormalities, within inflamed pulmonary vessels, lung parenchyma and reticulo-endothelial tissues, have an anti-viral or tissue repair role, or whether being activated as part of the wider immune response to virus they are themselves promoting vascular and tissue injury. The implications for opposing strategies to either boost or inhibit macrophage function are obvious, and necessitate urgent further investigation.

AJRCCM Articles in Press. Published November 20, 2020 as 10.1164/rccm.202008-3265OC

Fourth, plasma cell abnormalities in the reticuloendothelial system and lung provided further evidence of an aberrant host response in fatal COVID-19. While plasma cell expansion is expected to ensure production of antibody in the context of acute infections, the levels seen in our study were extremely marked. Plasma cells exhibited morphologic atypia but displayed a reactive, polytypic phenotype. To some extent this correlates with peripheral blood findings in patients with COVID-19 where $CD4^+$ and $CD8^+$ T-cell depletion is characteristic but B-cell numbers are maintained, with higher B-cell numbers reported in severe cases(40, 41). The plasma cells in our study were generally $MUM1^+$ and $CD38^+$ but CD138 (syndecan) low/negative raising the possibility that these are short-lived plasma cells or are at a transitional or arrested stage of development(42). In addition to macrophage behaviour and iron accumulation, this identifies plasma cells as a priority for future investigation of therapeutic targets.

This report has several limitations. We did not recruit non-COVID-19 patients into our cohort as this work was conducted as an urgent investigation into COVID-19, rather than to describe how COVID-19 differs from any other specific pulmonary/systemic disease or infection. Indeed, any immuno-pathological changes in COVID-19 that are shared with other causes of severe pulmonary injury/inflammation may still be avenues for therapeutic intervention. Reports of histological findings in fatal influenza provide some comparison as discussed above in the context of thrombosis, but we are unaware of a similar depth of pulmonary parenchymal immunophenotyping being reported.

AJRCCM Articles in Press. Published November 20, 2020 as 10.1164/rccm.202008-3265OC

The bone marrow B-cell and macrophage iron storage abnormalities reported here have not been observed in fatal influenza and may therefore be unique to COVID-19 (43, 44). The patient cohort is heterogeneous, in particular with respect to age, receipt of invasive mechanical ventilation (based on clinical escalation decisions) and receipt of experimental therapeutics (corticosteroids and azithromycin). Whilst we were unable to perform viral culture due to biosafety requirements we have partly mitigated this by identifying and sequence reads unique to viral subgenomic mRNA as an indicator of viral RNA synthesis. Viral RNA detection was performed by non-quantitative multiplex PCR but we recognise quantification of viral load using quantitative RT-PCR would yield potentially useful data. Finally, the histopathologists assessing tissue inflammation were not blinded to the diagnosis of COVID-19.

Taken together, these data provide comprehensive clinical, viral and immunological profiling of severe COVID-19. This highlights, for the first time, the discrepancy between the presence of SARS-CoV-2 and tissue inflammation. We conclude that death in COVID-19 occurs with a significant component of immune-mediated, rather than pathogen-mediated, organ inflammation and injury. This is consistent with the recent discovery that immunosuppression with corticosteroids prevents death in severe COVID-19, supporting virus-independent immunopathology being one of the primary mechanisms underlying fatal COVID-19. This suggests that better understanding of non-injurious, organ specific viral tolerance mechanisms and

AJRCCM Articles in Press. Published November 20, 2020 as 10.1164/rccm.202008-3265OC

targeting of the dysregulated immune response merits further investigation in COVID-19.

**ACKNOWLEDGEMENTS**

ICECAP research depends on the generosity of donors and their families who provide the valuable gift of tissue after death.

**COMPETING INTEREST DECLARATION**

The authors declare no competing interests.

AJRCCM Articles in Press. Published November 20, 2020 as 10.1164/rccm.202008-3265OC

## REFERENCES

1. Smatti MK, Cyprian FS, Nasrallah GK, Al Thani AA, Almishal RO, Yassine HM. Viruses and Autoimmunity: A Review on the Potential Interaction and Molecular Mechanisms. *Viruses* 2019; 11: 762.

2. Medzhitov R, Schneider DS, Soares MP. Disease tolerance as a defense strategy. *Science* 2012; 335: 936-941.

3. Schneider DS, Ayres JS. Two ways to survive infection: what resistance and tolerance can teach us about treating infectious diseases. *Nat Rev Immunol* 2008; 8: 889-895.

4. Glass EJ. The molecular pathways underlying host resistance and tolerance to pathogens. *Front Genet* 2012; 3: 263.

5. Mehta P, McAuley DF, Brown M, Sanchez E, Tattersall RS, Manson JJ. COVID-19: consider cytokine storm syndromes and immunosuppression. *Lancet* 2020; 395: 1033-1034.

6. Mehta P, Porter JC, Manson JJ, Isaacs JD, Openshaw PJM, McInnes IB, Summers C, Chambers RC. Therapeutic blockade of granulocyte macrophage colony-stimulating factor in COVID-19-associated hyperinflammation: challenges and opportunities. *The Lancet Respiratory Medicine*.

AJRCCM Articles in Press. Published November 20, 2020 as 10.1164/rccm.202008-3265OC

7. McElvaney OJ, McEvoy NL, McElvaney OF, Carroll TP, Murphy MP, Dunlea DM, O NC, Clarke J, O'Connor E, Hogan G, Ryan D, Sulaiman I, Gunaratnam C, Branagan P, O'Brien ME, Morgan RK, Costello RW, Hurley K, Walsh S, de Barra E, McNally C, McConkey S, Boland F, Galvin S, Kiernan F, O'Rourke J, Dwyer R, Power M, Geoghegan P, Larkin C, O'Leary RA, Freeman J, Gaffney A, Marsh B, Curley GF, McElvaney NG. Characterization of the Inflammatory Response to Severe COVID-19 Illness. *Am J Respir Crit Care Med* 2020; 202: 812-821.

8. Docherty AB, Harrison EM, Green CA, Hardwick HE, Pius R, Norman L, Holden KA, Read JM, Dondelinger F, Carson G, Merson L, Lee J, Plotkin D, Sigfrid L, Halpin S, Jackson C, Gamble C, Horby PW, Nguyen-Van-Tam JS, Ho A, Russell CD, Dunning J, Openshaw PJM, Baillie JK, Semple MG. Features of 20 133 UK patients in hospital with COVID-19 using the ISARIC WHO Clinical Characterisation Protocol: prospective observational cohort study. *BMJ* 2020; 369.

9. Cummings MJ, Baldwin MR, Abrams D, Jacobson SD, Meyer BJ, Balough EM, Aaron JG, Claassen J, Rabbani LE, Hastie J, Hochman BR, Salazar-Schicchi J, Yip NH, Brodie D, O'Donnell MR. Epidemiology, clinical course, and outcomes of critically ill adults with COVID-19 in New York City: a prospective cohort study. *Lancet* 2020.

AJRCCM Articles in Press. Published November 20, 2020 as 10.1164/rccm.202008-3265OC

10. Richardson S, Hirsch JS, Narasimhan M, Crawford JM, McGinn T, Davidson KW, Barnaby DP, Becker LB, Chelico JD, Cohen SL, Cookingham J, Coppa K, Diefenbach MA, Dominello AJ, Duer-Hefele J, Falzon L, Gitlin J, Hajizadeh N, Harvin TG, Hirschwerk DA, Kim EJ, Kozel ZM, Marrast LM, Mogavero JN, Osorio GA, Qiu M, Zanos TP. Presenting Characteristics, Comorbidities, and Outcomes Among 5700 Patients Hospitalized With COVID-19 in the New York City Area. *JAMA* 2020.

11. Zhou F, Yu T, Du R, Fan G, Liu Y, Liu Z, Xiang J, Wang Y, Song B, Gu X, Guan L, Wei Y, Li H, Wu X, Xu J, Tu S, Zhang Y, Chen H, Cao B. Clinical course and risk factors for mortality of adult inpatients with COVID-19 in Wuhan, China: a retrospective cohort study. *Lancet* 2020; 395: 1054-1062.

12. Horby P, Lim WS, Emberson J, Mafham M, Bell J, Linsell L, Staplin N, Brightling C, Ustianowski A, Elmahi E, Prudon B, Green C, Felton T, Chadwick D, Rege K, Fegan C, Chappell LC, Faust SN, Jaki T, Jeffery K, Montgomery A, Rowan K, Juszczak E, Baillie JK, Haynes R, Landray MJ. Effect of Dexamethasone in Hospitalized Patients with COVID-19: Preliminary Report. *medRxiv* 2020: 2020.2006.2022.20137273.

13. Sterne JAC, Murthy S, Diaz JV, Slutsky AS, Villar J, Angus DC, Annane D, Azevedo LCP, Berwanger O, Cavalcanti AB, Dequin PF, Du B, Emberson J, Fisher D, Giraudeau B, Gordon AC, Granholm A, Green C, Haynes R, Heming N,

AJRCCM Articles in Press. Published November 20, 2020 as 10.1164/rccm.202008-3265OC

Higgins JPT, Horby P, Jüni P, Landray MJ, Le Gouge A, Leclerc M, Lim WS, Machado FR, McArthur C, Meziani F, Møller MH, Perner A, Petersen MW, Savovic J, Tomazini B, Veiga VC, Webb S, Marshall JC. Association Between Administration of Systemic Corticosteroids and Mortality Among Critically Ill Patients With COVID-19: A Meta-analysis. *JAMA* 2020.

14. Wilk AJ, Rustagi A, Zhao NQ, Roque J, Martínez-Colón GJ, McKechnie JL, Ivison GT, Ranganath T, Vergara R, Hollis T, Simpson LJ, Grant P, Subramanian A, Rogers AJ, Blish CA. A single-cell atlas of the peripheral immune response in patients with severe COVID-19. *Nature Medicine* 2020; 26: 1070-1076.

15. Liao M, Liu Y, Yuan J, Wen Y, Xu G, Zhao J, Cheng L, Li J, Wang X, Wang F, Liu L, Amit I, Zhang S, Zhang Z. Single-cell landscape of bronchoalveolar immune cells in patients with COVID-19. *Nature Medicine* 2020: 1-3.

16. Puelles VG, Lütgehetmann M, Lindenmeyer MT, Sperhake JP, Wong MN, Allweiss L, Chilla S, Heinemann A, Wanner N, Liu S, Braun F, Lu S, Pfefferle S, Schröder AS, Edler C, Gross O, Glatzel M, Wichmann D, Wiech T, Kluge S, Pueschel K, Aepfelbacher M, Huber TB. Multiorgan and Renal Tropism of SARS-CoV-2. *New England Journal of Medicine* 2020.

17. Gupta A, Madhavan MV, Sehgal K, Nair N, Mahajan S, Sehrawat TS, Bikdeli B, Ahluwalia N, Ausiello JC, Wan EY, Freedberg DE, Kirtane AJ, Parikh SA, Maurer MS, Nordvig AS, Accili D, Bathon JM, Mohan S, Bauer KA, Leon MB,

AJRCCM Articles in Press. Published November 20, 2020 as 10.1164/rccm.202008-3265OC

Krumholz HM, Uriel N, Mehra MR, Elkind MSV, Stone GW, Schwartz A, Ho DD, Bilezikian JP, Landry DW. Extrapulmonary manifestations of COVID-19. *Nat Med* 2020.

18. Dorward DA, Russell CD, Um IH, Elshani M, Armstrong SD, Penrice-Randal R, Millar T, Lerpiniere CE, Tagliavini G, Hartley CS, Randall NP, Gachanja NN, Potey PM, Anderson AM, Campbell VL, Duguid AJ, Al Qsous W, BouHaidar R, Baillie JK, Dhaliwal K, Wallace WA, Bellamy CO, Prost S, Smith C, Hiscox JA, Harrison DJ, Lucas CD. Tissue-specific tolerance in fatal COVID-19. *medRxiv* 2020: 2020.2007.2002.20145003.

19. Hsia CC, Hyde DM, Ochs M, Weibel ER. An official research policy statement of the American Thoracic Society/European Respiratory Society: standards for quantitative assessment of lung structure. *Am J Respir Crit Care Med* 2010; 181: 394-418.

20. Sungnak W, Huang N, Bécavin C, Berg M, Queen R, Litvinukova M, Talavera-López C, Maatz H, Reichart D, Sampaziotis F, Worlock KB, Yoshida M, Barnes JL, Banovich NE, Barbry P, Brazma A, Collin J, Desai TJ, Duong TE, Eickelberg O, Falk C, Farzan M, Glass I, Gupta RK, Haniffa M, Horvath P, Hubner N, Hung D, Kaminski N, Krasnow M, Kropski JA, Kuhnemund M, Lako M, Lee H, Leroy S, Linnarson S, Lundeberg J, Meyer KB, Miao Z, Misharin AV, Nawijn MC, Nikolic MZ, Noseda M, Ordovas-Montanes J, Oudit GY, Pe'er D, Powell

AJRCCM Articles in Press. Published November 20, 2020 as 10.1164/rccm.202008-3265OC

J, Quake S, Rajagopal J, Tata PR, Rawlins EL, Regev A, Reyfman PA, Rozenblatt-Rosen O, Saeb-Parsy K, Samakovlis C, Schiller HB, Schultze JL, Seibold MA, Seidman CE, Seidman JG, Shalek AK, Shepherd D, Spence J, Spira A, Sun X, Teichmann SA, Theis FJ, Tsankov AM, Vallier L, van den Berge M, Whitsett J, Xavier R, Xu Y, Zaragosi L-E, Zerti D, Zhang H, Zhang K, Rojas M, Figueiredo F, Network HCALB. SARS-CoV-2 entry factors are highly expressed in nasal epithelial cells together with innate immune genes. *Nature Medicine* 2020; 26: 681-687.

21. Hou YJ, Okuda K, Edwards CE, Martinez DR, Asakura T, Dinnon KH, 3rd, Kato T, Lee RE, Yount BL, Mascenik TM, Chen G, Olivier KN, Ghio A, Tse LV, Leist SR, Gralinski LE, Schäfer A, Dang H, Gilmore R, Nakano S, Sun L, Fulcher ML, Livraghi-Butrico A, Nicely NI, Cameron M, Cameron C, Kelvin DJ, de Silva A, Margolis DM, Markmann A, Bartelt L, Zumwalt R, Martinez FJ, Salvatore SP, Borczuk A, Tata PR, Sontake V, Kimple A, Jaspers I, O'Neal WK, Randell SH, Boucher RC, Baric RS. SARS-CoV-2 Reverse Genetics Reveals a Variable Infection Gradient in the Respiratory Tract. *Cell* 2020.

22. Cifuentes-Muñoz N, Dutch RE, Cattaneo R. Direct cell-to-cell transmission of respiratory viruses: The fast lanes. *PLoS Pathog* 2018; 14: e1007015.

AJRCCM Articles in Press. Published November 20, 2020 as 10.1164/rccm.202008-3265OC

23. Yang YL, Meng F, Qin P, Herrler G, Huang YW, Tang YD. Trypsin promotes porcine deltacoronavirus mediating cell-to-cell fusion in a cell type-dependent manner. *Emerg Microbes Infect* 2020; 9: 457-468.

24. Nicholls JM, Poon LL, Lee KC, Ng WF, Lai ST, Leung CY, Chu CM, Hui PK, Mak KL, Lim W, Yan KW, Chan KH, Tsang NC, Guan Y, Yuen KY, Peiris JS. Lung pathology of fatal severe acute respiratory syndrome. *Lancet* 2003; 361: 1773-1778.

25. Gu J, Gong E, Zhang B, Zheng J, Gao Z, Zhong Y, Zou W, Zhan J, Wang S, Xie Z, Zhuang H, Wu B, Zhong H, Shao H, Fang W, Gao D, Pei F, Li X, He Z, Xu D, Shi X, Anderson VM, Leong AS. Multiple organ infection and the pathogenesis of SARS. *J Exp Med* 2005; 202: 415-424.

26. Raj GD, Jones RC. Infectious bronchitis virus: Immunopathogenesis of infection in the chicken. *Avian Pathol* 1997; 26: 677-706.

27. Snow TA, Singer M, Arulkumaran N. Immunomodulators in COVID-19 - Two Sides to Every Coin. *Am J Respir Crit Care Med* 2020.

28. Zhou F, Yu T, Du R, Fan G, Liu Y, Liu Z, Xiang J, Wang Y, Song B, Gu X, Guan L, Wei Y, Li H, Wu X, Xu J, Tu S, Zhang Y, Chen H, Cao B. Clinical course and risk factors for mortality of adult inpatients with COVID-19 in Wuhan, China: a retrospective cohort study. *The Lancet* 2020; 395: 1054-1062.

AJRCCM Articles in Press. Published November 20, 2020 as 10.1164/rccm.202008-3265OC

29. Drakesmith H, Prentice A. Viral infection and iron metabolism. *Nature Reviews Microbiology* 2008; 6: 541-552.

30. Ackermann M, Verleden SE, Kuehnel M, Haverich A, Welte T, Laenger F, Vanstapel A, Werlein C, Stark H, Tzankov A, Li WW, Li VW, Mentzer SJ, Jonigk D. Pulmonary Vascular Endothelialitis, Thrombosis, and Angiogenesis in COVID-19. *New England Journal of Medicine* 2020; 0: null.

31. Menter T, Haslbauer JD, Nienhold R, Savic S, Hopfer H, Deigendesch N, Frank S, Turek D, Willi N, Pargger H, Bassetti S, Leuppi JD, Cathomas G, Tolnay M, Mertz KD, Tzankov A. Post-mortem examination of COVID19 patients reveals diffuse alveolar damage with severe capillary congestion and variegated findings of lungs and other organs suggesting vascular dysfunction. *Histopathology*; n/a.

32. Patel BV, Arachchillage DJ, Ridge CA, Bianchi P, Doyle JF, Garfield B, Ledot S, Morgan C, Passariello M, Price S, Singh S, Thakuria L, Trenfield S, Trimlett R, Weaver C, Wort SJ, Xu T, Padley SPG, Devaraj A, Desai SR. Pulmonary Angiopathy in Severe COVID-19: Physiologic, Imaging, and Hematologic Observations. *Am J Respir Crit Care Med* 2020; 202: 690-699.

33. Hwang DM, Chamberlain DW, Poutanen SM, Low DE, Asa SL, Butany J. Pulmonary pathology of severe acute respiratory syndrome in Toronto. *Mod Pathol* 2005; 18: 1-10.

AJRCCM Articles in Press. Published November 20, 2020 as 10.1164/rccm.202008-3265OC

34. Gill JR, Sheng ZM, Ely SF, Guinee DG, Beasley MB, Suh J, Deshpande C, Mollura DJ, Morens DM, Bray M, Travis WD, Taubenberger JK. Pulmonary pathologic findings of fatal 2009 pandemic influenza A/H1N1 viral infections. *Arch Pathol Lab Med* 2010; 134: 235-243.

35. Mauad T, Hajjar LA, Callegari GD, da Silva LF, Schout D, Galas FR, Alves VA, Malheiros DM, Auler JO, Jr., Ferreira AF, Borsato MR, Bezerra SM, Gutierrez PS, Caldini ET, Pasqualucci CA, Dolhnikoff M, Saldiva PH. Lung pathology in fatal novel human influenza A (H1N1) infection. *Am J Respir Crit Care Med* 2010; 181: 72-79.

36. Carvelli J, Demaria O, Vély F, Batista L, Benmansour NC, Fares J, Carpentier S, Thibult ML, Morel A, Remark R, André P, Represa A, Piperoglou C, Cordier PY, Le Dault E, Guervilly C, Simeone P, Gainnier M, Morel Y, Ebbo M, Schleinitz N, Vivier E. Association of COVID-19 inflammation with activation of the C5a-C5aR1 axis. *Nature* 2020.

37. Zelek WM, Cole J, Ponsford MJ, Harrison RA, Schroeder BE, Webb N, Jolles S, Fegan C, Morgan M, Wise MP, Morgan BP. Complement Inhibition with the C5 Blocker LFG316 in Severe COVID-19. *Am J Respir Crit Care Med* 2020.

38. Zhao Y, Qin L, Zhang P, Li K, Liang L, Sun J, Xu B, Dai Y, Li X, Zhang C, Peng Y, Feng Y, Li A, Hu Z, Xiang H, Ogg G, Ho L-P, McMichael A, Jin R, Knight JC,

AJRCCM Articles in Press. Published November 20, 2020 as 10.1164/rccm.202008-3265OC

Dong T, Zhang Y. Longitudinal COVID-19 profiling associates IL-1RA and IL-10 with disease severity and RANTES with mild disease. *JCI Insight* 2020; 5.

39. De Luca G, Cavalli G, Campochiaro C, Della-Torre E, Angelillo P, Tomelleri A, Boffini N, Tentori S, Mette F, Farina N, Rovere-Querini P, Ruggeri A, D'Aliberti T, Scarpellini P, Landoni G, De Cobelli F, Paolini JF, Zangrillo A, Tresoldi M, Trapnell BC, Ciceri F, Dagna L. GM-CSF blockade with mavrilimumab in severe COVID-19 pneumonia and systemic hyperinflammation: a single-centre, prospective cohort study. *The Lancet Rheumatology* 2020; 2: e465-e473.

40. Chen G, Wu D, Guo W, Cao Y, Huang D, Wang H, Wang T, Zhang X, Chen H, Yu H, Zhang X, Zhang M, Wu S, Song J, Chen T, Han M, Li S, Luo X, Zhao J, Ning Q. Clinical and immunological features of severe and moderate coronavirus disease 2019. *The Journal of Clinical Investigation* 2020; 130: 2620-2629.

41. Mathew D, Giles JR, Baxter AE, Greenplate AR, Wu JE, Alanio C, Oldridge DA, Kuri-Cervantes L, Pampena MB, D'Andrea K, Manne S, Chen Z, Huang YJ, Reilly JP, Weisman AR, Ittner CAG, Kuthuru O, Dougherty J, Nzingha K, Han N, Kim J, Pattekar A, Goodwin EC, Anderson EM, Weirick ME, Gouma S, Arevalo CP, Bolton MJ, Chen F, Lacey SF, Hensley SE, Apostolidis S, Huang AC, Vella LA, Betts MR, Meyer NJ, Wherry EJ. Deep immune profiling of COVID-19 patients reveals patient heterogeneity and distinct immunotypes

AJRCCM Articles in Press. Published November 20, 2020 as 10.1164/rccm.202008-3265OC

with implications for therapeutic interventions. *bioRxiv* 2020: 2020.2005.2020.106401.

42. O'Connor BP, Raman VS, Erickson LD, Cook WJ, Weaver LK, Ahonen C, Lin LL, Mantchev GT, Bram RJ, Noelle RJ. BCMA is essential for the survival of long-lived bone marrow plasma cells. *J Exp Med* 2004; 199: 91-98.

43. Harms PW, Schmidt LA, Smith LB, Newton DW, Pletneva MA, Walters LL, Tomlins SA, Fisher-Hubbard A, Napolitano LM, Park PK, Blaivas M, Fantone J, Myers JL, Jentzen JM. Autopsy findings in eight patients with fatal H1N1 influenza. *Am J Clin Pathol* 2010; 134: 27-35.

44. Yu L, Wang Z, Chen Y, Ding W, Jia H, Chan JF-W, To KK-W, Chen H, Yang Y, Liang W, Zheng S, Yao H, Yang S, Cao H, Dai X, Zhao H, Li J, Bao Q, Chen P, Hou X, Li L, Yuen K-Y. Clinical, Virological, and Histopathological Manifestations of Fatal Human Infections by Avian Influenza A(H7N9) Virus. *Clinical Infectious Diseases* 2013; 57: 1449-1457.

AJRCCM Articles in Press. Published November 20, 2020 as 10.1164/rccm.202008-3265OC

## FIGURE LEGENDS

**Figure 1. Mapping SARS-CoV-2 organotropism and cellular distribution in fatal COVID-19 in relation to tissue inflammation.**

(**A**) Distribution of SARS-CoV-2 RNA for all patients was determined by multiplex PCR (colour intensity denotes frequency of detectable RNA, dotted line on legend denotes maximal frequency within the patient cohort) (n=11). Extent of organ-specific inflammation was assessed semi-quantitatively (0-3; no inflammation (0) to severe inflammatory changes (3)) with aggregate scores visualised (n=11). (B) Distribution of individual patient viral RNA presence within organs plotted against time interval between illness onset and death compared with organ specific inflammation scores for each patient. (C-D) Multiplex PCR positive samples were confirmed by sequencing, with (**C**) the proportion of the SARS-CoV-2 genome mapped calculated and (**D**) a representative sequence coverage map of the respiratory tract of one patient shown. (E-F) Tissue and cellular distribution of SARS-CoV-2 S protein was evaluated by immunohistochemistry and multiplex immunofluorescence on randomly selected SARS-CoV-2 PCR-positive FFPE tissue (n=4 patients). (E) Representative images demonstrate the tissue distribution of S protein within nasal mucosal, bronchial epithelium, small bowel enterocytes, distal biliary epithelium within the liver and distal renal tubular epithelium; scale bar = 50 micrometers. (**F**) Within the lung, cellular localization of S protein is demonstrated within the alveolar epithelium (AE1/3) and rarely in macrophages (CD68) and endothelium (CD105) within the lung parenchyma.

AJRCCM Articles in Press. Published November 20, 2020 as 10.1164/rccm.202008-3265OC

**Figure 2. Delineating pulmonary injury and vascular involvement in fatal COVID-19.**

(**A**) Detailed spatial evaluation of lung injury and key pathological abnormalities were determined within each lobe of lung for each patient (A-K) and compared with the presence or absence of SARS-CoV-2 viral RNA by multiplex PCR (*denotes invasive mechanical ventilation, n=11). LUL-left upper lobe, LLL-left lower lobe, RUL-right upper lobe, RML-right middle lobe, RLL-right lower lobe. Representative images of organising and exudative diffuse alveolar damage, pulmonary thrombus, bronchopneumonia, uninflamed lung, and variable inflammation within the same lung. (**B**) In four individuals frequent pulmonary vasculature immune infiltration was seen, with (**C**) multiplex immunofluorescence defining these immune cell populations (CD4, CD8 (T cells); CD20 (B cells); CD68 (macrophages); MRP8 (neutrophils and myeloid lineage cells)) demonstrating MRP8 immunopositive mononuclear cells to be the predominant cell type (representative image, white stars denotes vessel lumen and white dashed line denotes elastic lamina) scale bar = 200 micrometers. (**D)** Analysis of 50 arteries/arterioles from two selected patients quantifying cell types involved in vasculitis.

**Figure 3. Pulmonary tissue and reticulo-endothelial immune responses to fatal COVID-19.**

Regions of interest were defined by histological examination of H&E stained lung tissue to identify areas of diffuse alveolar damage (DAD) in tissue from five patients

AJRCCM Articles in Press. Published November 20, 2020 as 10.1164/rccm.202008-3265OC

(**A**: representative image). Corresponding multiplex immunofluorescence defined vascular endothelium (CD34) relative to immune cell populations: CD4, CD8 (T cells); CD20 (B cells); CD68 (macrophages); MRP8 (neutrophils and myeloid lineage cells) (**B**) with and (**C**) without autofluorescence scale bar = 200 micrometers. Separate cell populations are highlighted in panels **D**-**E**. Immune cell populations were quantified, with (**F**) relative abundance of cell types compared between COVID-19 (n=5) and normal, uninflamed lung from patients undergoing lung cancer resection (n=4) and (**G**) spatially stratified into vascular/perivascular and parenchymal regions. (**H**) Key pathological abnormalities within bone marrow included erythroid dysplasia, iron-laden macrophages and haemophagocytosis; plasma cells were confirmed by immunohistochemical staining and quantified in bone marrow aspirates. (**I**) Representative image of bone marrow aspirate analysis demonstrating erythroid dysplasia (white arrows) and frequent plasma cells (red arrows). (**J**) Mismatch between stereotyped plasma cell abnormalities in spleen and mediastinal lymph node (LN) (red) and detection of SARS-CoV-2 by multiplex PCR (green: PCR-positive; grey: PCR-negative).

AJRCCM Articles in Press. Published November 20, 2020 as 10.1164/rccm.202008-3265OC

**TABLE**

| | **n=11** |
|---|---|
| Age, y | 76.8 ±11.7 |
| Sex, M/F | 10/1 |
| Illness duration, d | 23.6 ± 10.0 |
| | |
| Clinical & radiological features | |
| Hypoxic respiratory failure | 11 (100) |
| Bacterial pneumonia | |
| Microbiologically-confirmed | 4 (36.4) |
| Suspected | 6 (54.5) |
| Thoracic radiology | |
| Pulmonary GGO | 11 (100) |
| Pulmonary embolism | 3 (27.3) |
| | |
| Supportive care | |
| Supplemental oxygen | 11 (100) |
| Invasive mechanical ventilation | 4 (36.4) |
| Duration, d* | 18.3 ± 7.8 |
| Vasopressors | 4 (36.4) |
| Renal replacement therapy | 3 (27.3) |

Abbreviations: GGO = ground glass opacification; CRP = C-reactive protein.
*time from intubation to death.
Data are presented as mean ± SD or absolute number (% of total).

AJRCCM Articles in Press. Published November 20, 2020 as 10.1164/rccm.202008-3265OC

# Figure 1.

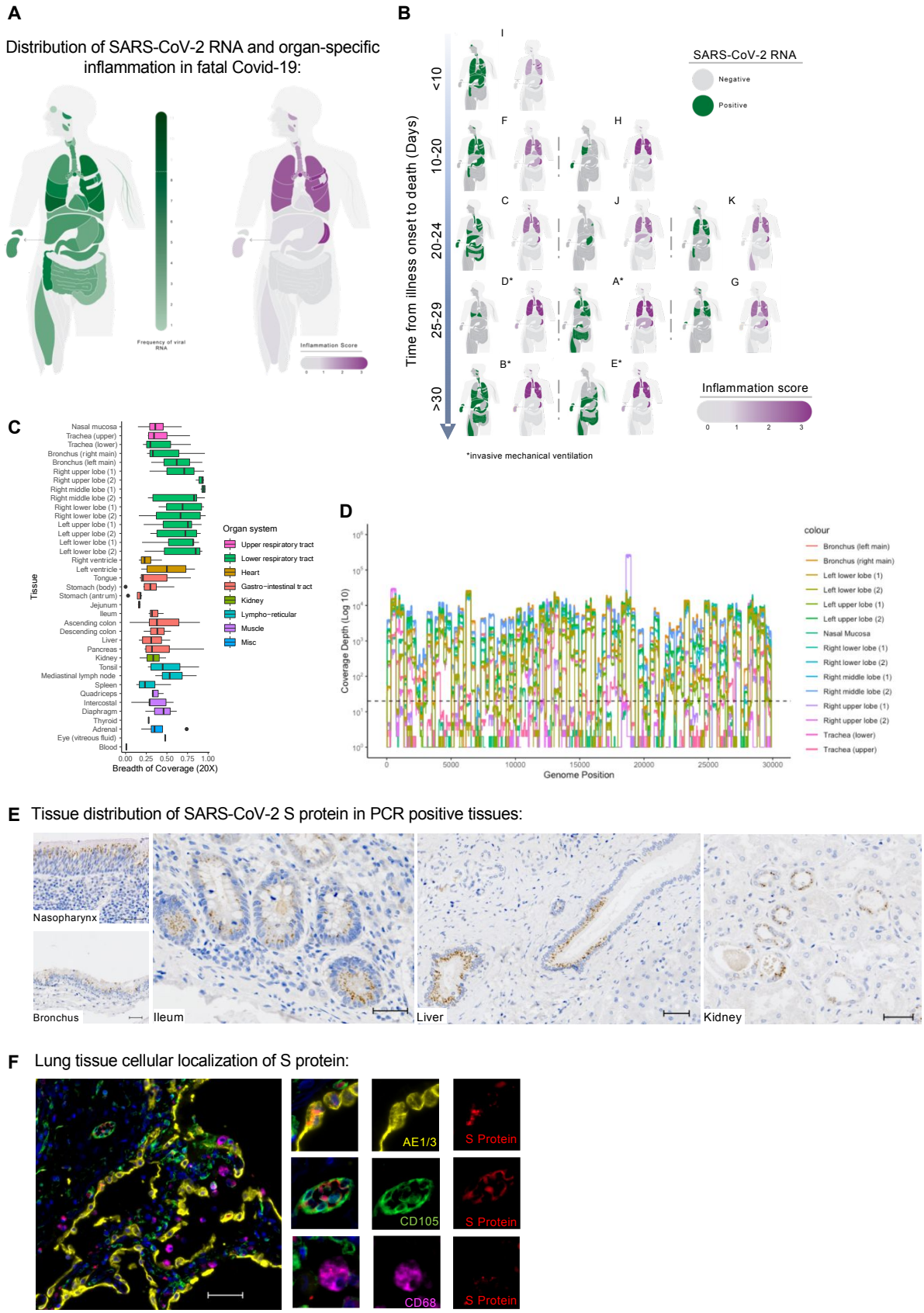


AJRCCM Articles in Press. Published November 20, 2020 as 10.1164/rccm.202008-3265OC

**Figure 2.**

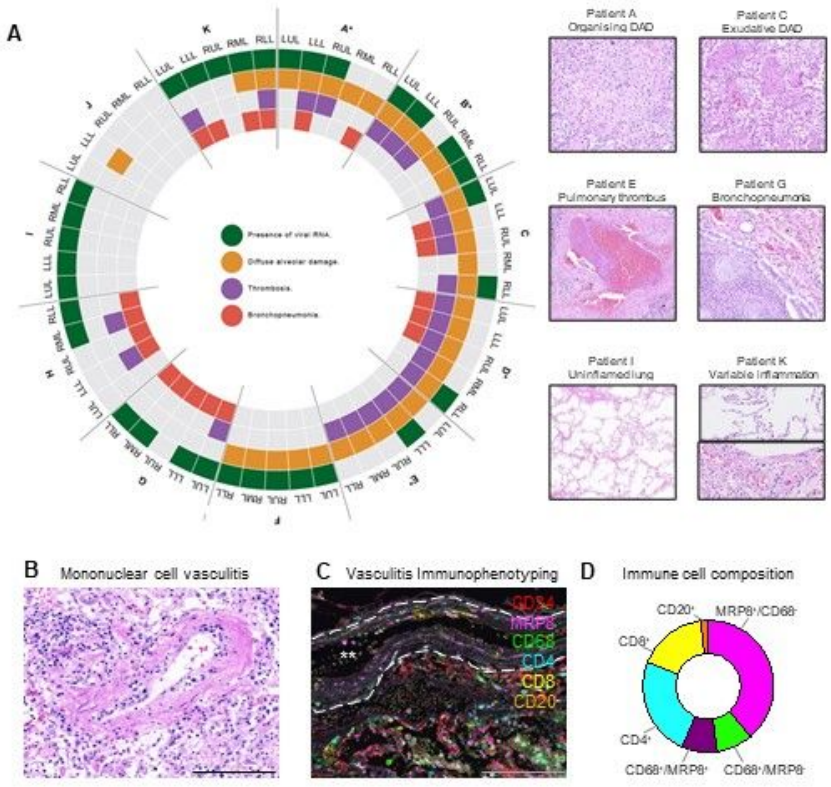


AJRCCM Articles in Press. Published November 20, 2020 as 10.1164/rccm.202008-3265OC

**Figure 3.**

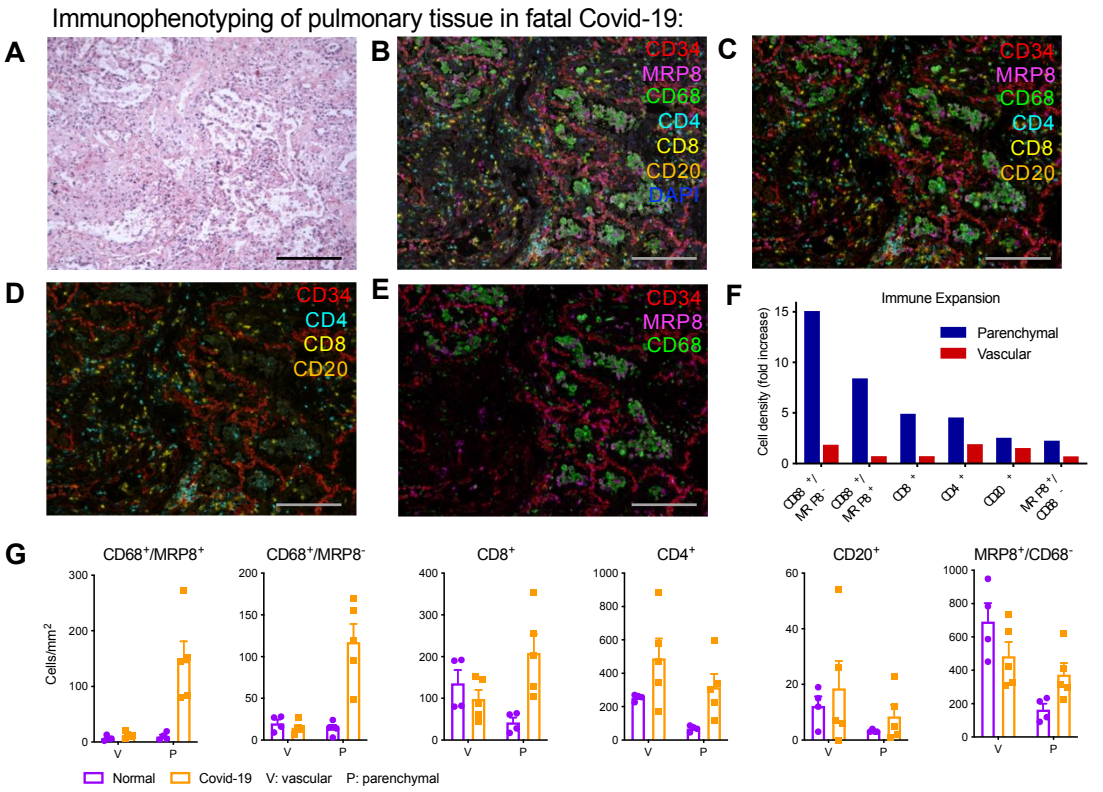


AJRCCM Articles in Press. Published November 20, 2020 as 10.1164/rccm.202008-3265OC

# Tissue-specific Immunopathology in Fatal Covid-19

David A Dorward, Clark D Russell, In Hwa Um, Mustafa Elshani, Stuart D Armstrong, Rebekah Penrice-Randal, Tracey Millar, Chris EB Lerpiniere, Giulia Tagliavini, Catherine S Hartley, Nadine P. Randle, Naomi N Gachanja, Philippe MD Potey, Xiaofeng Dong, Alison M Anderson, Victoria L Campbell, Alasdair J Duguid, Wael Al Qsous, Ralph BouHaidar, J Kenneth Baillie, Kevin Dhaliwal, William A Wallace, Christopher OC Bellamy, Sandrine Prost, Colin Smith, Julian A Hiscox, David J Harrison, Christopher D Lucas on behalf of the ICECAP consortium.

## Online Data Supplement

### Table of Contents





AJRCCM Articles in Press. Published November 20, 2020 as 10.1164/rccm.202008-3265OC

AJRCCM Articles in Press. Published November 20, 2020 as 10.1164/rccm.202008-3265OC

## ICECAP consortium members

*Principal Investigators*

David A Dorward, University of Edinburgh Centre for Inflammation Research
Christopher D Lucas, University of Edinburgh Centre for Inflammation Research
Clark D Russell, University of Edinburgh Centre for Inflammation Research
J Kenneth Baillie, Roslin Institute, University of Edinburgh
David J Harrison, School of Medicine, University of St Andrews

*Clinical*

Chris EB Lerpiniere, Centre for Clinical Brain Sciences, University of Edinburgh
Lorna C Mackintosh, Department of Pathology, Royal Infirmary of Edinburgh
Tracey Millar, Centre for Clinical Brain Sciences, University of Edinburgh
Charles TA Parker, Department of Pathology, Royal Infirmary of Edinburgh
Prasad P Velu, University of Edinburgh Centre for Inflammation Research
Irene AF Young, University of Edinburgh Centre for Inflammation Research

*Clinical Pathology*

Wael Al Qsous, Department of Pathology, Western General Hospital, Edinburgh
Alison M Anderson, Mortuary Department, Royal Infirmary of Edinburgh
Christopher OC Bellamy, Department of Pathology, Royal Infirmary of Edinburgh
Ralph BouHaidar, Department of Pathology, Royal Infirmary of Edinburgh
John Greenwood, Mortuary Department, Royal Infirmary of Edinburgh
Jennifer Haynes, Mortuary Department, Royal Infirmary of Edinburgh
Leanne C Knapp, Mortuary Department, Royal Infirmary of Edinburgh
Anca Oniscu, Department of Pathology, Royal Infirmary of Edinburgh
David N Poller, Department of Pathology, Queen Alexandra Hospital, Portsmouth
David M Reilly, Mortuary Department, Royal Infirmary of Edinburgh
Mary N Sheppard, Cardiovascular Pathology Unit, St George's Medical School, London
Colin Smith, Centre for Clinical Brain Sciences, University of Edinburgh
William A Wallace, Department of Pathology, Royal Infirmary of Edinburgh
David K Worrall, Department of Pathology, Western General Hospital, Edinburgh

*Data Visualization & Graphic Design*

Markos Spyrides, Department of Architecture & Civil Engineering, University of Bath

*Hematology*

Victoria L Campbell, Department of Haematology, Western General Hospital
Alasdair J Duguid, Department of Haematology, Western General Hospital

*Laboratory Pathology*



AJRCCM Articles in Press. Published November 20, 2020 as 10.1164/rccm.202008-3265OC

Mustafa Elshani, School of Medicine, University of St Andrews
In Hwa Um, School of Medicine, University of St Andrews
Sandrine Prost, University of Edinburgh Centre for Inflammation Research
Giuliana Tagliavini, University of Edinburgh Centre for Inflammation Research

*Radiology*
John T Murchison, Department of Radiology, Royal Infirmary of Edinburgh

*Respiratory Medicine*
Kevin Dhaliwal, University of Edinburgh Centre for Inflammation Research

*Laboratory Science*
Naomi N Gachanja, University of Edinburgh Centre for Inflammation Research
Beth Henderson, University of Edinburgh Centre for Inflammation Research
Philippe MD Potey, University of Edinburgh Centre for Inflammation Research
Emma J Scholefield, University of Edinburgh Centre for Inflammation Research

*Virology*
Julian A Hiscox, Institute of Infection, Veterinary & Ecological Sciences, University of Liverpool
Mai M Almsaud, Institute of Infection, Veterinary & Ecological Sciences, University of Liverpool
Muhannad Alruwaili, Veterinary & Ecological Sciences, University of Liverpool
Abdulrahman Alrezaihi, Institute of Infection, Veterinary & Ecological Sciences, University of Liverpool
Stuart D Armstrong, Institute of Infection, Veterinary & Ecological Sciences, University of Liverpool
Eleanor G Bentley, Institute of Infection, Veterinary & Ecological Sciences, University of Liverpool
Jordan J Clark, Institute of Infection, Veterinary & Ecological Sciences, University of Liverpool
Xiaofeng Dong, Institute of Infection, Veterinary & Ecological Sciences, University of Liverpool
Isabel Garcia-Dorival, Institute of Infection, Veterinary & Ecological Sciences, University of Liverpool
Paul KF Gilmore, Institute of Infection, Veterinary & Ecological Sciences, University of Liverpool
Ximeng Han, Institute of Infection, Veterinary & Ecological Sciences, University of Liverpool
Catherine Hartley, Institute of Infection, Veterinary & Ecological Sciences, University of Liverpool
Benjamin Jones, Institute of Infection, Veterinary & Ecological Sciences, University of Liverpool
Lisa Luu, Institute of Infection, Veterinary & Ecological Sciences, University of Liverpool
Shona Moore, Institute of Infection, Veterinary & Ecological Sciences, University of Liverpool
Rebekah Penrice-Randal, Institute of Infection, Veterinary & Ecological Sciences, University of Liverpool
Nadine P Randle, Institute of Infection, Veterinary & Ecological Sciences, University of Liverpool
Parul Sharma, Institute of Infection, Veterinary & Ecological Sciences, University of Liverpool
Ghada T Shawli, Institute of Infection, Veterinary & Ecological Sciences, University of Liverpool
James P Stewart, Institute of Infection, Veterinary & Ecological Sciences, University of Liverpool
Lance Turtle, Institute of Infection, Veterinary & Ecological Sciences, University of Liverpool



AJRCCM Articles in Press. Published November 20, 2020 as 10.1164/rccm.202008-3265OC

## CRediT statement

*DAD, CDL, CDR, JKB, DJH, JAH, CS:* Conceptualization, Methodology, Validation, Formal analysis, Investigation, Data Curation, Writing – Original Draft, Writing – Review & Editing, Visualization, Supervision, Project administration, Funding acquisition. *CEBL, LCM, TM, CTAP, PPV, WQA, COCB, RB, AO, DNP, DMR, MS, WAW, DKW, VLC, AJD, ME, SP, IHU, JTM, GT, MMA, AA, SDA, EGB, JJC, IG-D, PKFG, XD, CH, BJ, LL, RP-R, NPR, PS, GTS, JPS:* Investigation, Formal analysis. *IAFY, NNG:* Data Curation. *KD, AMA, JG, JH, LCK, NNG, BH, EJS, LT, SM:* Resources. *MS, PMDP:* Visualization



AJRCCM Articles in Press. Published November 20, 2020 as 10.1164/rccm.202008-3265OC

## Supplementary Methods

### Post-mortem examinations

Patients with pre-mortem PCR-confirmed SARS-CoV-2 infection and evidence of lower respiratory tract disease, who were considered to be approaching the end of life, were referred to the research team by their responsible clinician. After death, authorization for a hospital post-mortem and collection of tissues and data for research was requested from the decedent's nearest relative. Royal College of Pathologists guidance on COVID-19 autopsies were followed (1). All staff wore personal protective equipment including FFP3 respirators and all post-mortem examinations were conducted within a high-risk facility. Representative samples were collected systematically, following a standardized sampling and fixation protocol, from the vitreous, blood, posterior nasal mucosa, posterior base of tongue, tonsil, thyroid, trachea (upper and lower), bronchi (right and left main), sub-carinal/peri-hilar mediastinal lymph nodes, lung (all five lobes), heart (right and left ventricle), liver, kidney, spleen, pancreas, adrenal, stomach, jejunum, ileum, colon (ascending and descending) and muscle (quadriceps, diaphragm and intercostal) (Supplementary Fig. 1). Bone marrow aspirate (1ml) and trephine were taken from the anterior aspect of the right ribs. Brain tissue was not sampled due to local health and safety arrangements.

### Histopathological analysis

Sample processing followed a standardised pipeline in the hospital diagnostic pathology laboratory (2). Following haematoxylin and eosin staining of tissue, additional special stains and immunohistochemistry were performed as required for clinical diagnostics. Bone marrow trephine samples were decalcified in EDTA prior to processing. Bone marrow aspirates were collected in EDTA then smear and squash preparations were prepared, fixed and stained with Wright-Giemsa and Perl's. Bone marrow cellularity was assessed at 10x power and morphological assessment was performed at 50x. A minimum of 1000 nucleated cells were counted to assess hematopoietic activity, proportions of cell lineages, morphology and iron storage. Organ histology was reviewed by a group of expert organ-specific histopathologists (WAW, DAD, COCB, WAQ, AO, MS, DNP, DKW). Formal reports were written for each case and subsequently semi-quantitatively scored based on the degree of acute organ injury and inflammation (for each: none=0, mild=1, moderate=2, severe=3) and absence or presence (a or b respectively) of pre-existing chronic change. Acute lung injury scoring incorporated features of diffuse alveolar damage and bronchopneumonia. Other organs were scored for features of acute necro-inflammatory injury while spleen and lymph node scores were based on the extent of aberrant morphological features.

### Multiplex immunofluorescence

FFPE slides were de-paraffinized and rehydrated. Endogenous peroxidase was blocked with 3% $H_2O_2$ for 30 mins. Antigen retrieval was performed in a decloaking chamber (BioCare) at 110ºC for 30 mins in EDTA (0.175mM pH 8) followed by cooling and rinsing with water then PBS. Slides were then incubated with the primary antibody at indicated concentrations (Supplementary Table 5) for 30 mins at room temperature (or overnight at 4ºC for CD68), followed by Opal polymer HRP-conjugated secondary antibody for 30 mins, then with the chosen Opal (Akoya) fluorophore (1:100) for 10 mins. Each step was followed by washes with PBS. Microwave treatment in EDTA (0.175mM), for 15 mins once boiling, was used for antibody removal between steps and this was repeated as required for multiplex staining. Slides were then incubated in DAPI for 5 mins at room temperature, rinsed with PBS and water, then mounted with ProLong™ Diamond (Invitrogen). Images were captured using a Vectra Polaris slide scanner (Akoya Biociences). A whole slide scan at x20 resolution was used to select regions of interest for multi-spectral scanning, with an average of 40 fields (931x698μm) per section (40x resolution using objective 0.75NA at 2x2 binning). Single colour staining done in parallel with the experiment was used to build a specific spectral library (Supplementary Fig. 5) allowing optimum spectral un-mixing of the fluorophores and



AJRCCM Articles in Press. Published November 20, 2020 as 10.1164/rccm.202008-3265OC

phenotyping analysis. Images were analysed using inForm 2.9.5 with (i) trainable tissue segmentation on autofluorescence, DAPI and CD34, with medium pattern, extra fine segmentation resolution and trimming edges by 4 pixels and (ii) adaptable cell segmentation with DAPI as a nuclear marker (minimum size 30 μm, splitting sensitivity of 0.77) and CD8, CD4 and MRP8 as assisting membrane stains (nuclear splitting sensitivity of 1.58), and phenotyping in layers ($CD4^+$, $CD8^+$, $CD20^+$, $MRP8^+/CD68^+$). Complex phenotypes ($CD68^{+/-}$, $MRP8^{+/-}$) were analysed using PhenopTR (akoyabio.github.io/phenoptr/) in R (package version 0.2.7). Statistical analysis was performed in Minitab 19 Statistical Software (2019, State College, Pennsylvania).

Primary antibody concentrations were optimized using 3,3'-diaminobenzidine chromogen-based staining, followed by single colour immunofluorescence with one fluorophore to assess the relative intensities of the markers. All markers were then allocated a fluorophore according to intensity to achieve a balanced intensity over all the fluorophores. The antibodies and concentrations used are shown in Table S6. Assessment of inflammatory cell infiltration into vessel walls was performed in 50 arterial profiles from two patients with approximately 900 cells phenotyped. Archived uninflamed lung tissue was obtained from background lung tissue taken at the time of lung cancer resection through NHS Lothian BioResource SR419.

**RNA extraction and SARS-CoV-2 PCR**

TRIzol treated tissue samples were placed into 2 ml tissue homogenizing CKMix tubes (Precellys®) containing 1 ml of TRIzol reagent (Invitrogen). Samples were homogenized using a Bead Mill 24 Homogenizer (Thermofisher) at 4 m/s for 1 min. Samples were stored at -80°C until further processing. RNA extraction was performed according to the manufacturer's instructions (Invitrogen) using GlycoBlue™ co-precipitant (Thermofisher) to maximize yields. Directly following extraction, samples were DNase treated using TURBO™ DNase (Thermofisher) as per manufacturer's instructions. RNA concentration and quality were assessed using a Nanodrop One spectrophotometer (Thermofisher). RNA reverse transcription and PCR steps were carried out essentially as described in the protocol published by the ARTIC Network (2). Reverse transcription used SuperScript IV reverse transcriptase (Invitrogen) to generate single strand cDNA using a random primer mix (NEB, a mixture of random hexamers and anchored dT primer). The ARTIC primer set multiplex (v3), made up of 98 primer pairs, was used to create tiled PCR amplicons across the SARS-CoV-2 viral cDNA. Reaction conditions were: denaturation at 98°C for 30 sec followed by 40 cycles of 15 sec denaturation at 98°C; 5 min annealing and extension at 65°C; final hold at 4°C. Agarose gel analysis (1.5% gel, 1x TBE, 1x SYBR Safe DNA stain, run for 30 min at 110 V) was performed for verification of PCR products (ARTIC primers approximately 400bp) for every sample and each multiplex pool. Samples that were positive for SARS-CoV-2 were referred for sequencing.

**SARS-CoV-2 genome sequencing and bioinformatic analysis**

The PCR products from pool 1 and pool 2 ARTIC multiplex reactions for each sample were pooled and purified using AMPure XP beads (Beckman Coulter). Quantification of the amplicon pools before normalization was performed using a Qubit 4 fluorometer (Thermofisher). 50 ng of purified PCR product was end-prepared with Ultra II End repair/dA-tailing Module (NEB) and incubated at 20°C for 5 mins then 65°C for 5 mins. Nanopore native barcodes (EXP-NBD104/114) were ligated to end-prepared DNA using Ultra II Ligation Module (NEB) and incubated at 20°C for 20 mins then 65°C for 10 mins. Up to 24 barcoded samples were pooled and purified with AMPure XP beads (Beckman Coulter). Sequencing adapters were ligated to the barcoded library using the Quick Ligation Module (NEB) and incubated at room temperature for 20 mins. The sequencing library was purified once more with AMPure XP beads, eluted and loaded on a FLO-MIN106D flow cell for sequencing using Oxford Nanopore MinION or GridION based platforms. Minimap2 was used to align fastq sequences to the SARS-CoV-2 isolate Wuhan-Hu-1 reference genome (NC_045512.2) using the -ax map-ont parameters. Samtools was used to sort and index alignment files, and Picard was used to mark duplicates. A custom script written in



AJRCCM Articles in Press. Published November 20, 2020 as 10.1164/rccm.202008-3265OC

perl, was used to determine viral genome coverage which was then visualised in RStudio. Genome coverage for every PCR-positive sample is shown in Fig. S4.

**Detection of SARS-CoV-2 S protein by immunohistochemistry**

2.5µm thick FFPE sections were cut and dewaxed in bond dewax solution for 30 secs at 72°C then rehydrated in absolute alcohol then bond wash buffer. Antigen retrieval was performed with ER1 buffer (pH 6) at 100°C for 20 mins followed by rinsing in wash buffer then peroxidase blocking for 7 mins (BOND Polymer Refine Detection, Leica). Sections were incubated with anti-SARS S protein antibody (Abcam, clone number 3A2, catalogue number ab272420) diluted 1:500 in antibody diluent (Agilent) for 30 mins then rinsed with wash buffer. Post primary, polymer, DAB chromogen, then haematoxylin counterstain incubation steps were performed (BOND Polymer Refine Detection, Leica) and sections were dehydrated in alcohol then cleared in xylene prior to mounting. Whole slide images of brightfield and fluorescence slides were digitized using a Zeiss Axio Scan.Z1 scanner (Zeiss Microscopy) through a Plan-Apochromat 20x/0.8 M27 objective. Exposure times were set using a positive control tissue for a set of fluorescent probe panels and were kept constant across all slides stained using the named panel. Negative technical (no primary antibody) and biological (SARS-CoV-2 PCR-negative tissue) controls were included and tested. Isotype control showed complete negativity (Figure E9). A number of different SARS-CoV-2 spike glycoprotein antibodies were validated in house. Biological negative and positive control tissues, utilised for the antibody validation, were archival pre-Covid-19 autopsy lung tissue and current Covid19 PCR positive tissue, respectively. Moreover, a VERO cell line infected with SARS-CoV-2 virus (and uninfected control) were utilised to further validate the antibodies. For multiplexed immunofluorescence, primary antibodies used are listed in Table S6. Multiplexed scanned (whole slide imaging) images were imported into QuPath v0.2.0 (4). Individual cells were detected by the cell detection tool in QuPath using the hoechst channel. Single measurement classifiers were utilized to sub-classify AE1/3$^{+}$, CD105$^{+}$ and CD68$^{+}$ cells by the intensity of FITC, Cy3 and AF750 channels, respectively. In addition, S protein measurement classifier was set to distinguish its positivity in the Cy5 channel which was corroborated with IHC and subsequent negative controls. These single measurement classifiers were then combined into a composite classifier which measured the number of cells co-expressing AE1/3 and S protein, CD105 and S protein, and CD68 and S protein.



AJRCCM Articles in Press. Published November 20, 2020 as 10.1164/rccm.202008-3265OC

## Supplementary Figures

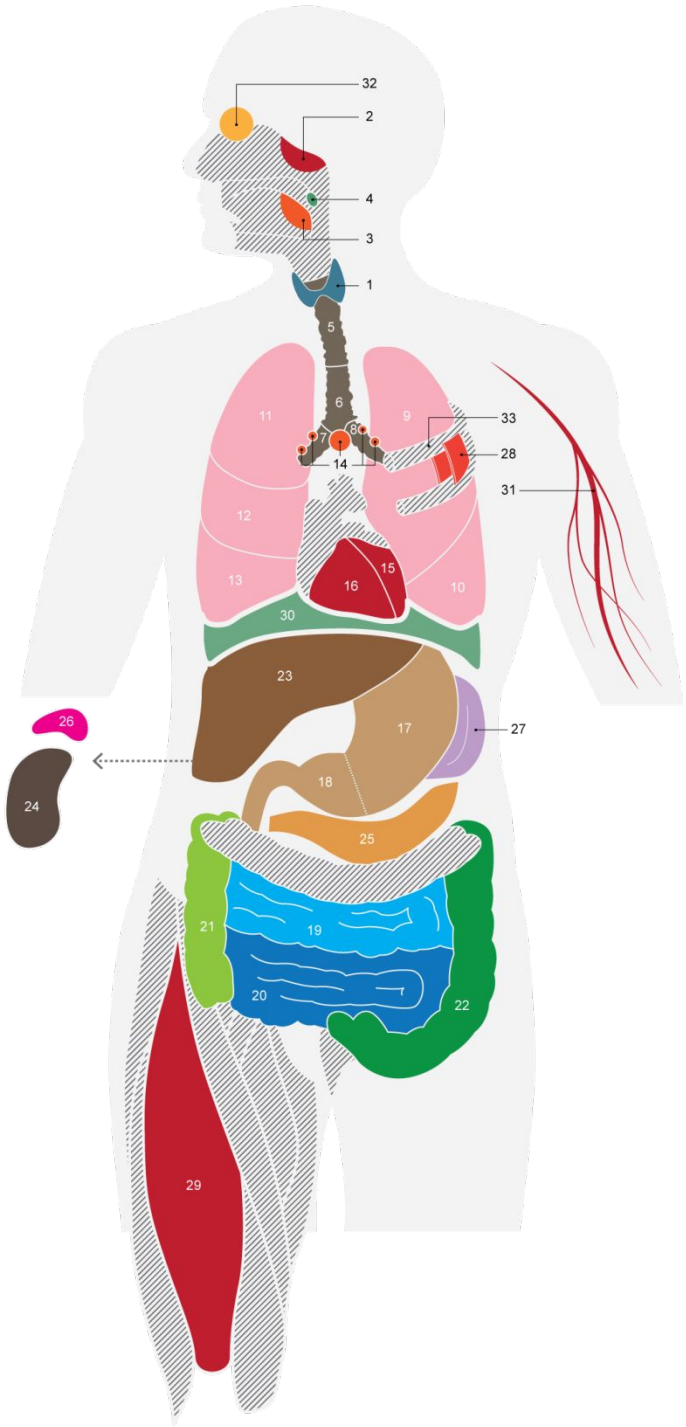


Key

| | |
|---|---|
| 1 | Thyroid |
| 2 | Nasal Mucosa |
| 3 | Tongue |
| 4 | Tonsil |
| 5 | Upper Trachea |
| 6 | Lower Trachea |
| 7 | Right Main Bronchus |
| 8 | Left Main Bronchus |
| 9 | Lungs • Left Upper Lobe (×3) |
| 10 | Lungs • Left Lower Lobe (×3) |
| 11 | Lungs • Right Upper Lobe (×3) |
| 12 | Lungs • Right Middle Lobe (×3) |
| 13 | Lungs • Right Lower Lobe (×3) |
| 14 | Mediastinal Lymph Node |
| 15 | Heart • Left Ventricle |
| 16 | Heart • Right Ventricle |
| 17 | Stomach Body |
| 18 | Stomach Antrum |
| 19 | Small Intestine • Jejenum |
| 20 | Small Intestine • Illeum |
| 21 | Large Intestine • Ascending |
| 22 | Large Intestine • Descending |
| 23 | Liver |
| 24 | Kidney |
| 25 | Pancreas |
| 26 | Adrenal Gland |
| 27 | Spleen |
| 28 | Intercoastal |
| 29 | Quadricep (Lateral) |
| 30 | Diaphragm |
| 31 | Blood |
| 32 | Vitreous Fluid |
| 33 | Bone Marrow |

**Figure E1. Schematic diagram of organs and tissues sampled at post-mortem.**



AJRCCM Articles in Press. Published November 20, 2020 as 10.1164/rccm.202008-3265OC

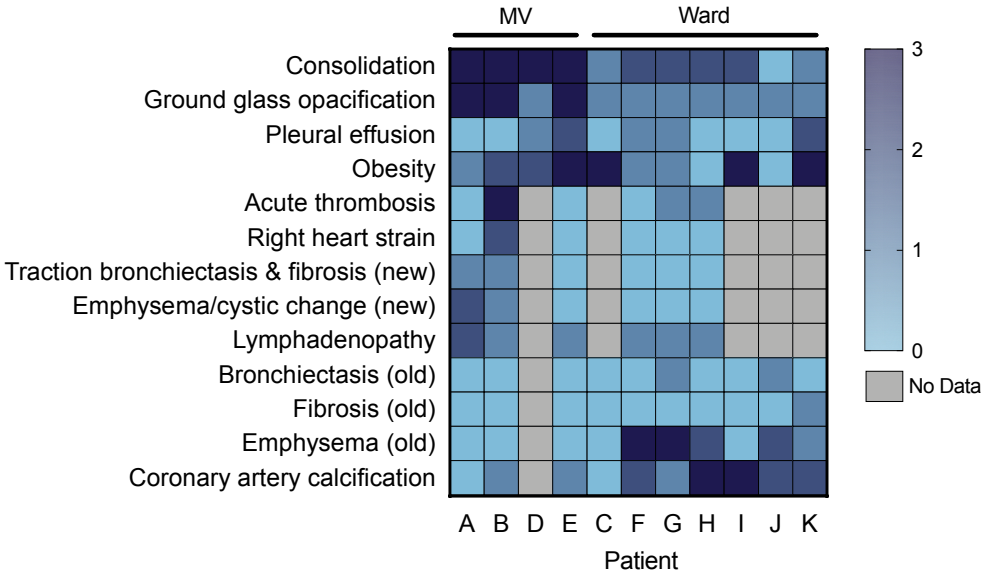


**Figure E2. Radiological findings in fatal Covid-19.**
Radiographic investigations and reports from all cases were reviewed by a multi-disciplinary team comprising thoracic radiologists, respiratory clinicians and specialist thoracic pathologists. Imaging was scored by a thoracic radiologist based on the presence (1=mild, 2=moderate, 3=severe) or absence (0) of relevant features. When cross-sectional imaging had not been performed during or shortly before the acute episode, any previous imaging was reviewed to identify pre-existing features such as emphysema, bronchiectasis, fibrosis or coronary artery calcification. Plain chest radiographs were available for all patients, demonstrating bilateral, peripheral, patchy consolidation or ground glass opacification of varying severity. Computed tomography pulmonary angiography (CTPA) was performed in five cases. In mechanically ventilated (MV) patients, features consistent with ARDS were apparent in addition to new cystic changes (cases A and B) and prominent basal bronchi with varicosities and traction (traction bronchiectasis), likely secondary to extensive consolidation but potentially due to the development of early fibrotic change (cases A, B, D). Pleural effusions, a less common radiologic feature of Covid-19 (5), were identified in 5/11 cases. Features of underlying respiratory or cardiac disease (emphysema, bronchiectasis, coronary artery calcification) were present in current and previous imaging of patients managed in the ward setting.

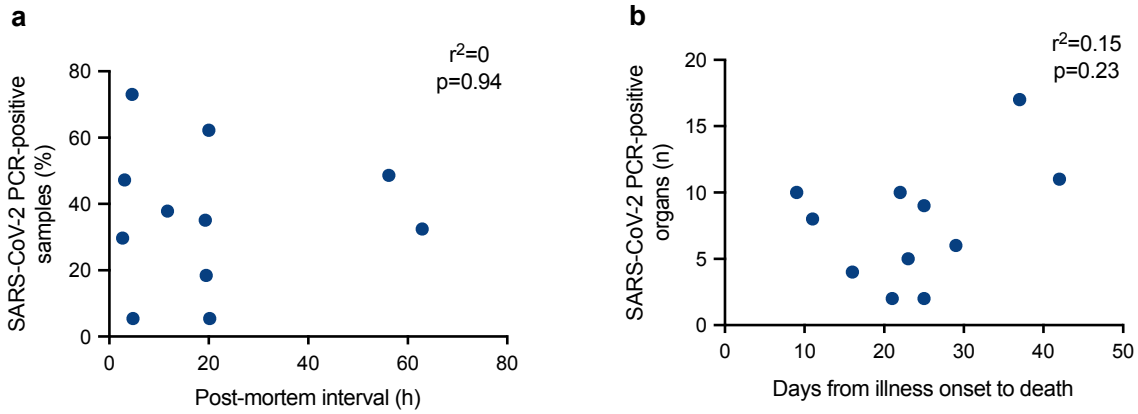


**Figure E3. No relationship between proportion of multiplex PCR-positive samples and time to post-mortem or time from illness onset to death.**



AJRCCM Articles in Press. Published November 20, 2020 as 10.1164/rccm.202008-3265OC

(**a**) The percentage of tissue samples obtained at post-mortem that tested positive by multiplex PCR post-mortem vs. the post-mortem interval, defined as the time from death to starting post-mortem examination, and (**b**) the number of PCR-positive organs vs. time from illness onset to death. Pearson correlation coefficient is shown



AJRCCM Articles in Press. Published November 20, 2020 as 10.1164/rccm.202008-3265OC

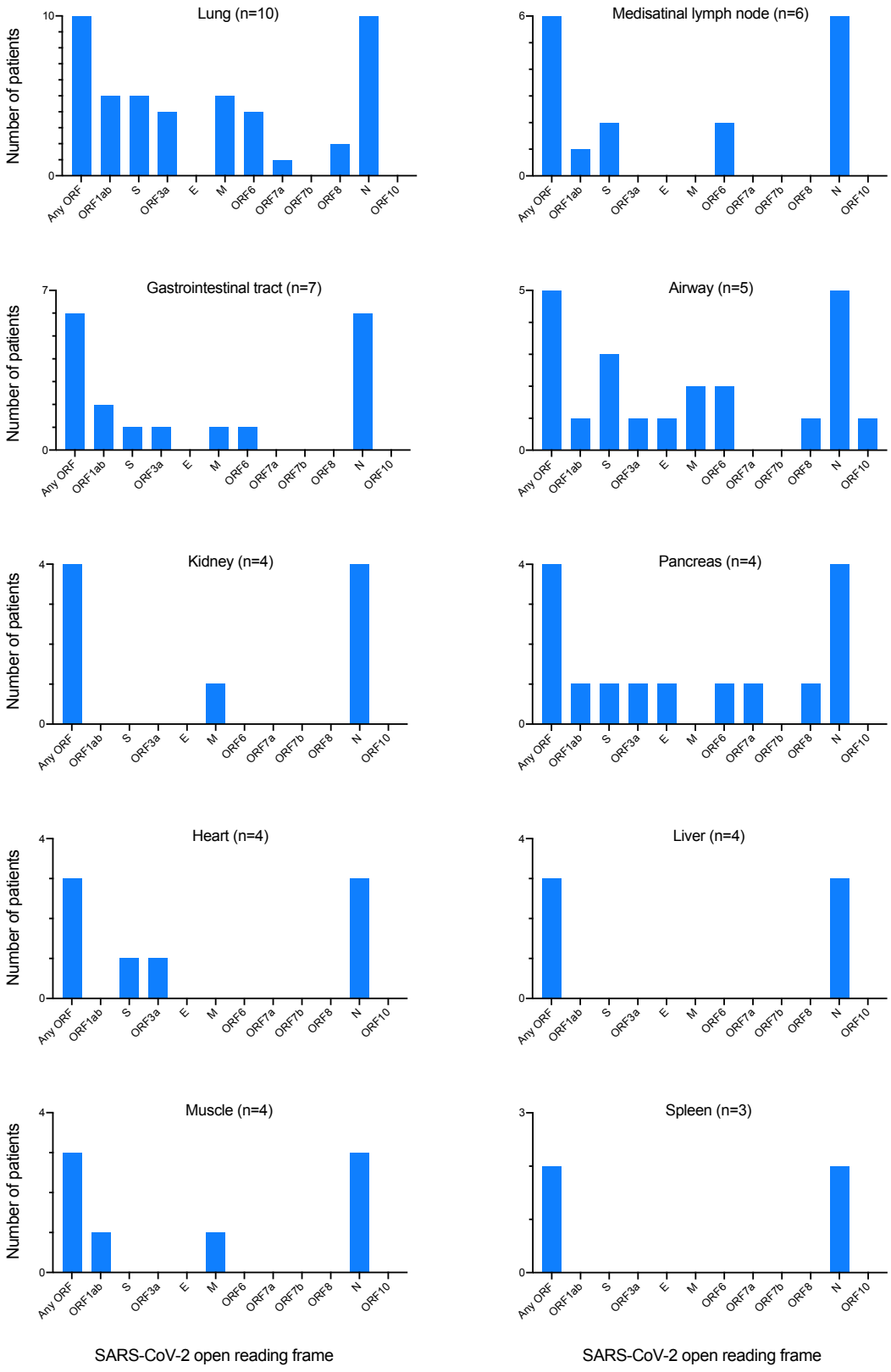


**Figure E4. SARS-CoV-2 subgenomic messenger RNA.**

Viral subgenomic mRNAs from each viral open reading frame were identified from sequencing reads of multiplex PCR products. The graphs show the presence/absence of subgenomic mRNA, indicative of active viral RNA synthesis, for specified anatomical sites. N refers to number of patients with PCR products available.



AJRCCM Articles in Press. Published November 20, 2020 as 10.1164/rccm.202008-3265OC

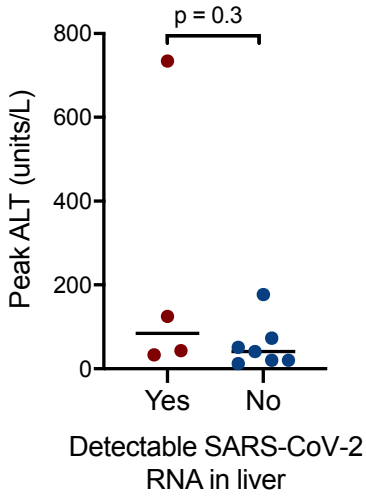


**Figure E5. Viral RNA detection in liver tissue and peak ALT.**
Presence or absence of SARS-CoV-2 in liver tissue vs. peak ALT. Bar represents median peak ALT measurement. Groups compared by Mann-Whitney test.

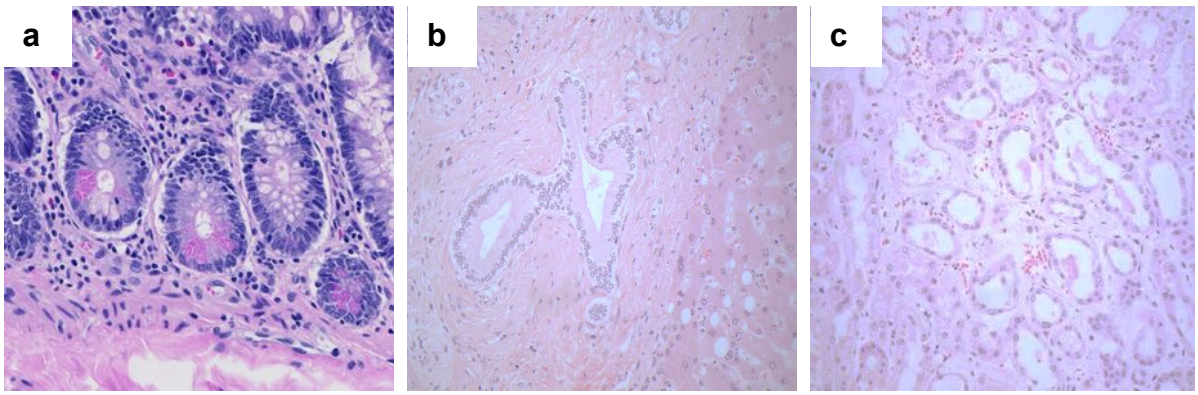


**Figure E6. Absence of inflammatory cell infiltrate in areas of ileum, liver and kidney that were positive for SARS-CoV-2 S protein.**
Corresponding H&E images of the same area within the tissue sections of (**a**) small intestine, (**b**) liver and (**c**) kidney displayed in Fig. 1. Images do not entirely overlap as multiple sections were taken between H&E and immunohistochemistry.



AJRCCM Articles in Press. Published November 20, 2020 as 10.1164/rccm.202008-3265OC

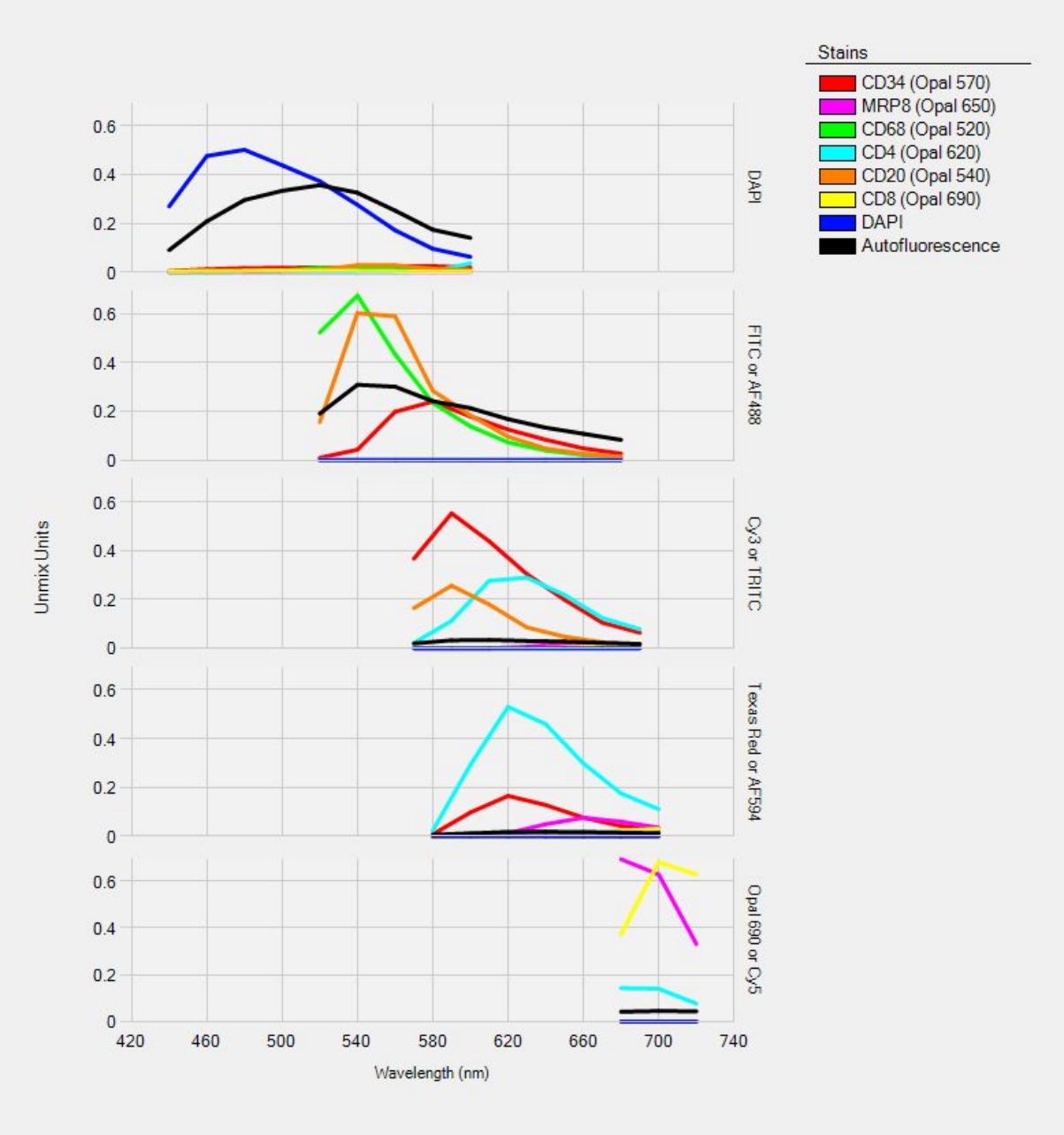


**Figure E7. Spectral library used for multiplex immunofluorescence images and data analyses in Figure 3.**



AJRCCM Articles in Press. Published November 20, 2020 as 10.1164/rccm.202008-3265OC

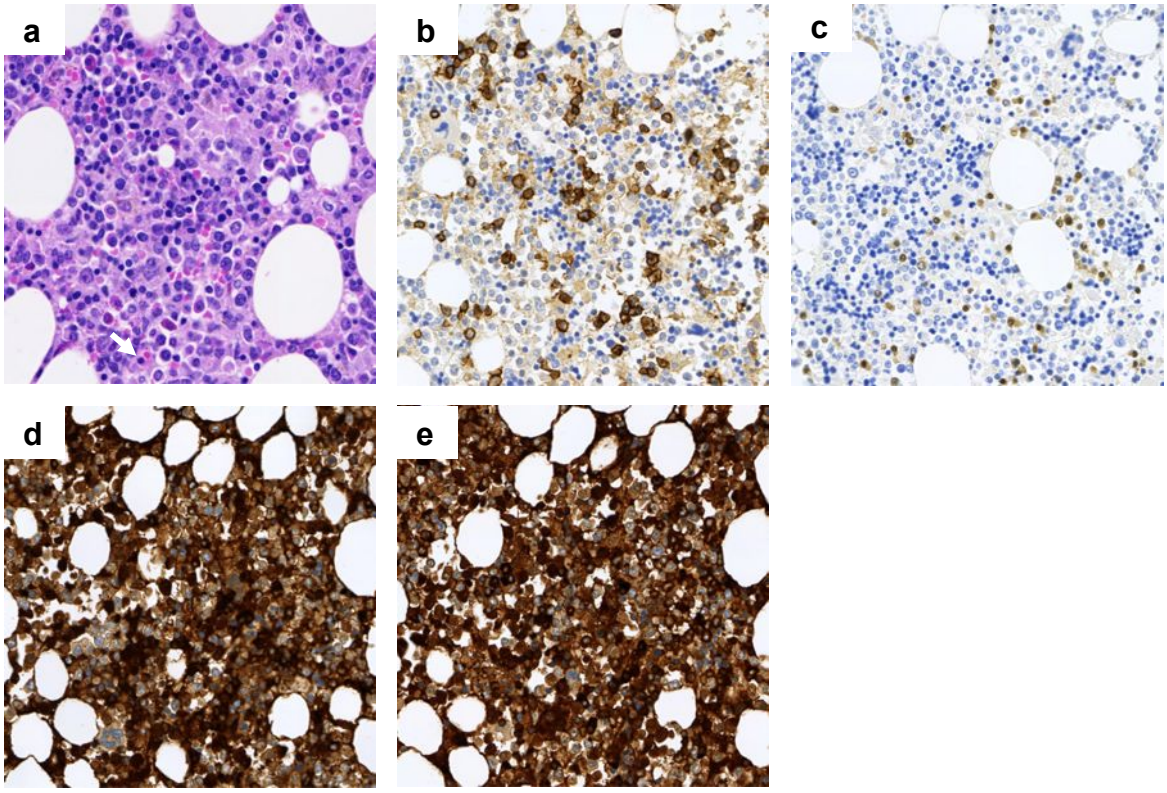


**Figure E8. Reticulo-endothelial responses in fatal Covid-19.**
Bone marrow trephine (**a**) confirmed the increased plasma cell number with immunohistochemical staining for (**b**) CD38 and (**c**) MUM1, with no evidence of a light chain restriction (**d**, lambda; **e**, kappa)

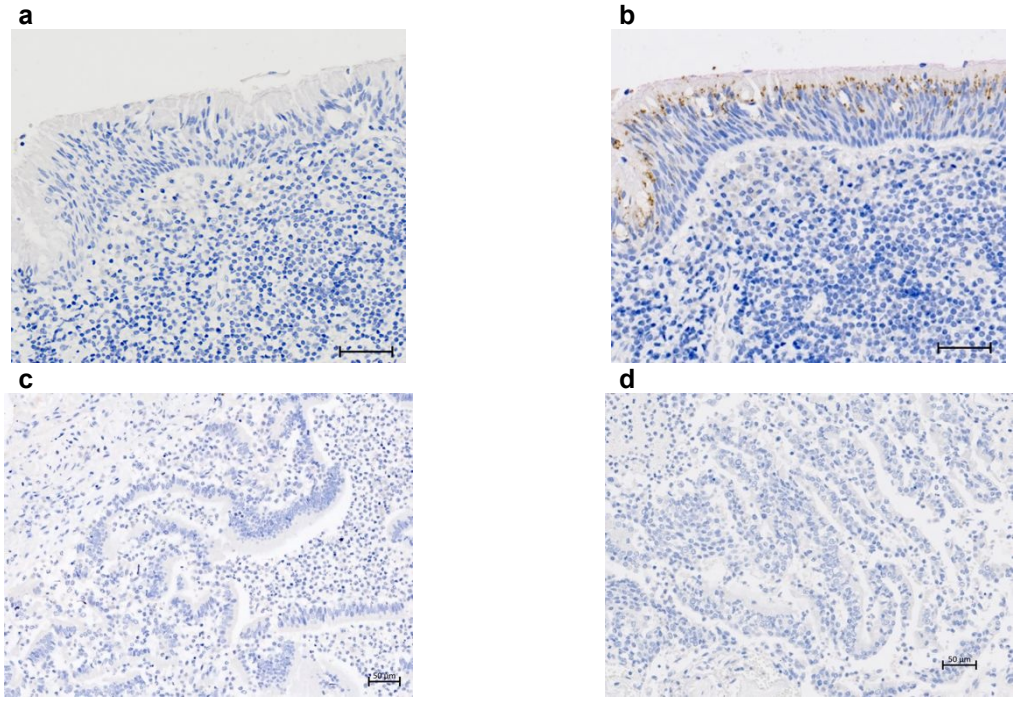


**Figure E9. Control samples used to validate S protein detection by immunohistochemistry.**



AJRCCM Articles in Press. Published November 20, 2020 as 10.1164/rccm.202008-3265OC

(**a**) Isotype control antibody and (**b**) anti-S protein antibody staining of nasopharyngeal tissue confirmed negativity for the isotype control. (**c**) and (**d**) show negative anti-S protein antibody staining of negative biological controls (lung tissue). Scale bar = 50 micrometers



AJRCCM Articles in Press. Published November 20, 2020 as 10.1164/rccm.202008-3265OC

## Supplementary Tables

### Table E1. Clinical details of included patients.

| Patient | Age, Sex | Past medical history | Symptoms* | | | Fever (≥38°C) | Illness duration (d)† | Supportive care | | | | Complications§ | Bacterial infection | Antimicrobials<br>Anticoagulants<br>Corticosteroids<br>Trial agents |
|---|---|---|---|---|---|---|---|---|---|---|---|---|---|---|
| | | | Respiratory | Enteric | Systemic | | | $O_2$ | IMV‡ | Vasopressors | RRT | | | |
| **A** | 66, M | CVD, hypothyroidism, psoriasis | + | + | + | + | 25 | + | + 19d | + | + | ARDS (P:F 89mmHg), AKI, impaired RV function | Confirmed VAP (BAL: *S. aureus* & *E. coli*) | Antimicrobials<br>Heparin SC (prophylaxis)<br>Corticosteroids |
| **B** | 67, M | Non-Hodgkin's lymphoma, in remission (rituximab) | + | – | + | + | 37 | + | + 12d | + | + | ARDS (P:F 205 mmHg), AKI, PE, impaired RV function | No | Antimicrobials<br>LMWH SC (therapeutic) |
| **C** | 72, M | COPD, PE, small cell lung cancer (6 years) | + | – | + | + | 22 | + | – | – | – | Pneumonitis | Confirmed HAP (sputum: coliforms & *H. influenzae*) | Antimicrobials<br>DOAC (previous PE)<br>Corticosteroids |
| **D** | 68, M | HTN | + | + | + | + | 25 | + | + 13d | + | – | ARDS (P:F 74mmHg) impaired RV function | Confirmed co-infection on admission (sputum: *S. aureus* & *S. pneumoniae*) | Antimicrobials<br>LMWH SC (prophylaxis) |
| **E** | 64, M | Sick sinus syndrome, CVD | + | – | + | + | 42 | + | + 29d | + | + | ARDS (P:F 82mmHg), AKI, vasopressor refractory shock | Confirmed VAP (BAL: *K. oxytoca*) | Antimicrobials<br>Heparin SC (prophylaxis)<br>Corticosteroids |
| **F** | 78, M | COPD, MGUS, post-mortem diagnosis B-cell lymphoma. | – | – | + | + | 11 | + | – | – | – | Pneumonitis, AKI | Suspected co-infection on admission | Antimicrobials |
| **G** | 84, F | PBC, COPD, recent PE | + | – | + | + | 29 | + | – | – | – | Pneumonitis, PE | Suspected HAP | Antimicrobials<br>LMWH SC (therapeutic)<br>Corticosteroids |
| **H** | 84, M | Dementia, AF, diverticulitis | + | – | – | – | 16 | + | – | – | – | Pneumonitis, PE | Suspected HAP | Antimicrobials<br>LMWH SC (therapeutic) |
| **I** | 70, M | Type 2 DM, HTN, IHD, CVD, dementia | + | – | + | + | 9 | + | – | – | – | Pneumonitis | Suspected HAP | Antimicrobials<br>LMWH SC (prophylaxis)<br>Azithromycin (trial) |



AJRCCM Articles in Press. Published November 20, 2020 as 10.1164/rccm.202008-3265OC

| | | | | | | | | | | | | | | |
|---|---|---|---|---|---|---|---|---|---|---|---|---|---|---|
| **J** | 97, M | IHD, COPD, HTN, AF, CKD, AS | + | + | – | + | 21 | + | – | – | – | Pneumonitis, AKI | Suspected HAP | Antimicrobials<br>LMWH SC (prophylaxis)<br>Corticosteroids |
| **K** | 95, M | CKD, HF, MGUS, AS | + | – | + | + | 23 | + | – | – | – | Pneumonitis, AKI | Suspected HAP | Antimicrobials<br>LMWH SC (prophylaxis) |

Patients had a mean age of 77 years (range 64–97), 10/11 were male, and the mean duration of symptoms prior to death was 24 days (range 9–42). All had pulmonary ground glass opacification on thoracic radiology indicative of viral pneumonitis. Four patients received mechanical ventilation (MV), for a mean of 18 days, and had a median P:F ratio of 86 mmHg prior to death, compatible with severe ARDS (6). Biochemical AKI (defined as increase in serum creatinine of 26.5μmol/L) or requirement for renal replacement therapy was present in 6/11 patients. Microbiologically confirmed (4/11) or clinically suspected (6/11) bacterial co- or secondary infection was common. HAP and VAP were diagnosed based on timing of onset relative to hospitalisation (HAP, >48h after admission) or intubation (VAP).

*_Respiratory_: respiratory symptoms (cough, sputum, sore throat, runny nose, ear pain, wheeze, chest pain); _Enteric_: gastrointestinal symptoms (abdominal pain, vomiting, diarrhoea); _Systemic_: systemic symptoms (myalgia, joint pain, fatigue). Symptom clusters defined by reference (7).

†Illness duration refers to time from symptom onset to death.

‡Duration for MV refers to time from intubation to death.

§P:F ratio calculated from results closest to time of death.

AF: atrial fibrillation; AKI: acute kidney injury; ARDS: acute respiratory distress syndrome; AS: aortic stenosis; BAL: bronchoalveolar lavage; COPD: chronic obstructive pulmonary disease; CKD: chronic kidney disease; CVD: cerebrovascular disease; DOAC: direct oral anticoagulant; DM: diabetes mellitus; HAP: hospital-acquired pneumonia; HF: heart failure; HTN: hypertension; IHD: ischemic heart disease; IMV: invasive mechanical ventilation; LMWH: low molecular weight heparin; MGUS: monoclonal gammopathy of uncertain significance; $O_2$: supplemental oxygen; PBC: primary biliary cirrhosis; PE: pulmonary embolism; RRT: renal replacement therapy; RV: right ventricle; SC: subcutaneous; VAP: ventilator-associated pneumonia.



AJRCCM Articles in Press. Published November 20, 2020 as 10.1164/rccm.202008-3265OC

**Table E2. Laboratory results closest to time of death.**

| Patient | **Hemoglobin,** g/L | **WCC,** x10⁹/L | **Neutrophils,** x10⁹/L | **Lymphocytes,** x10⁹/L | **Monocytes,** x10⁹/L | **Eosinophils,** x10⁹/L | **Platelets,** x10⁹/L | **Fibrinogen,** g/L | **PT,** secs | **APTT,** secs | **Urea,** mmol/L | **Creatinine,** µmol/L | **ALT,** units/L | **Bilirubin,** units/L | **CRP,** mg/L | **Maximum CRP,** mg/L |
|---|---|---|---|---|---|---|---|---|---|---|---|---|---|---|---|---|
| **A** | 79 | 15.4 | 12.7 | 0.5 | 0.3 | 0 | 216 | 3.5 | 13 | 30 | 9.5 | 102 | 30 | 17 | 134 | 272 |
| **B** | 89 | 11.7 | 10.4 | 0.3 | 0.68 | 0.29 | 204 | 7.6 | 14 | 36 | 7.3 | 81 | 734 | 24 | 243 | 243 |
| **C** | 144 | 7.5 | 6.84 | 0.39 | 0.2 | 0.01 | 89 | 6.7 | 21 | 36 | 10.3 | 82 | 33 | 11 | 126 | 270 |
| **D** | 95 | 28.4 | 25.45 | 1.58 | 1.12 | 0.21 | 643 | 5.8 | 17 | 27 | 9.6 | 57 | 51 | 10 | 258 | 318 |
| **E** | 71 | 12.4 | 8.92 | 1.62 | 1.4 | 0.33 | 348 | 6.2 | 12 | 27 | 8.9 | 159 | 31 | 14 | 356 | 371 |
| **F** | 106 | 6.4 | 5.78 | 0.45 | 0.17 | 0.01 | 180 | 5 | 16 | 41 | 12.1 | 146 | 41 | 8 | 242 | 242 |
| **G** | 69 | 9.4 | 7.5 | 0.64 | 1.26 | 0.01 | 370 | NA | NA | NA | 5.4 | 45 | 12 | 8 | 186 | 287 |
| **H** | 105 | 6.6 | 5.74 | 0.54 | 0.27 | 0.01 | 272 | 7 | 15 | 28 | 13.6 | 69 | 20 | 14 | 161 | 366 |
| **I** | 131 | 3.8 | 2.66 | 0.78 | 0.4 | 0.01 | 156 | NA | NA | NA | 5.1 | 67 | 41 | 19 | 91 | 91 |
| **J** | 113 | 14.6 | 13.39 | 0.69 | 0.48 | 0.01 | 272 | NA | NA | NA | 43.1 | 214 | 177 | 14 | 33 | 123 |
| **K** | 88 | 13.3 | 9.63 | 2.91 | 0.77 | 0.02 | 212 | 4.9 | 13 | 29 | 40.2 | 343 | 19 | 6 | 332 | 332 |
| Reference range | 115-160 | 4.0-11.0 | 2.0-7.5 | 1.4-4.0 | 0.2-0.8 | 0.04-0.4 | 150-400 | 1.5-4 | 10.5-13.5 | 26-36 | 2.5-6.6 | 50-98 | 10-50 | 3-21 | <5 | <5 |



AJRCCM Articles in Press. Published November 20, 2020 as 10.1164/rccm.202008-3265OC

**Table E3. Summary of kidney, liver, heart and muscle histological findings.**

| | N (n=11) |
|---|---|
| **Kidney** | |
| *Acute* | |
| Acute tubular injury | |
| Mild | 4 |
| Severe | 1 |
| Platelet/fibrin thrombus | 2 |
| Vasa recta leucocytosis with immature cells | |
| Frequent | 2 |
| Rare | 3 |
| Reactive podocyte changes | 1 |
| *Chronic* | |
| Arteriosclerosis | 11 |
| Severe | 9 |
| Interstitial fibrosis | 9 |
| **Liver** | |
| *Acute* | |
| Portal venopathy | 2 |
| Mild iron overload | 2 |
| Possible haemophagocytosis | 1 |
| Diffuse perivenular necrosis | 1 |
| Perivenular congestion & mild leucocytosis | 1 |
| *Chronic* | |
| Steatosis | 2 |
| Fibrosis | 2 |
| Steatohepatitis | 1 |
| Primary biliary cirrhosis | 1 |
| **Heart*** | |
| *Acute* | |
| Interstitial lymphocytes | 2 |
| Infarction | 1 |
| Platelet thrombi in vessels | 1 |
| Subendocardial thrombus | 1 |
| Haemorrhage | 1 |
| *Chronic* | |
| Fibrosis | 7 |
| Calcification | 1 |
| Nodular amyloid deposits | 1 |
| **Muscle*†** | |
| *Acute* | |
| Sparse inflammatory cell infiltrate | 6 |
| Contraction band necrosis (single cells) | 3 |
| *Chronic* | |
| Atrophy | 3 |



AJRCCM Articles in Press. Published November 20, 2020 as 10.1164/rccm.202008-3265OC

*n=10 for heart and muscle

†intercostal, diaphragm & quadriceps combined



AJRCCM Articles in Press. Published November 20, 2020 as 10.1164/rccm.202008-3265OC

**Table E4. Bone marrow abnormalities.**

| | Erythroid dysplasia[†] (% erythroid precursors) | | | | Plasma cells (% all nucleated cells[‡]) | | | | Iron laden macrophages | | | Haemophagocytosis |
|---|---|---|---|---|---|---|---|---|---|---|---|---|
| | –* | 0-10% | 10-50% | >50% | 0-5%* | 5-10% | >10% | Atypia[§] | –* | + | ++ | Present |
| **A** | | ✓ | | | ✓ | | | | | ✓ | | [(II)] |
| **B** | | | | ✓ | ✓ | | | | | | ✓ | ✓ |
| **C** | | | ✓ | | | | ✓ | ✓ | | | ✓ | |
| **D** | | ✓ | | | | | ✓ | ✓ | | | ✓ | |
| **E** | | | ✓ | | | | ✓ | ✓ | | ✓ | | |
| **G** | | ✓ | | | | ✓ | | ✓ | | ✓ | | ✓ |
| **H** | | | | ✓ | | ✓ | | ✓ | | ✓ | | ✓ |
| **I** | ✓ | | | | ✓ | | | | ✓ | | | |

– absent, + present, ++ increased

No assessable bone marrow aspirate material was available for patients F and J.

*indicates expected normal findings

[†]morphological abnormalities observed included nuclear blebs, multinucleated (bi- and tri-nucleated) early and late (primarily late) erythroblasts, defective haemoglobinization and megaloblastoid features

[‡]quantified from aspirate samples, where plasma cells were confirmed by immunohistochemical staining

[§,]morphologic abnormalities observed included bi- and tri-nucleated forms, immature forms, Russell bodies and Mott-like cells

[II]possible haemophagocytosis observed in liver

**Table E5. Primary antibodies used in immunofluorescence.**

| Antibody | Source | Concentration | Cellular target | Purpose |
|---|---|---|---|---|
| CD34 (Opal 570)* | Agilent, M716501-2 | 1:50 | Endothelial cells | Multiplex lung immune-phenotyping |
| MRP8 (Opal 690)* | Abcam, Ab219370 | 1:16000 | Myeloid lineages | |
| CD68 (Opal 520)* | DAKO, M0876 | 1:75 | Macrophages | |
| CD20 (Opal 540)* | Agilent, M075501-2 | 1:500 | B-cells | |
| CD8 (Opal 690)* | Leica, NCL-L-CD8-4B11 | 1:75 | T-cells | |
| CD4 (Opal 620)* | Abcam, Ab133616 | 1:400 | T-cells | |
| CD105 | Abcam, Ab114052 | 1:15000 | Endothelial cells | In situ analysis of viral spatial distribution |
| CD68 | Abcam, Ab213363 | 1:8000 | Macrophages | |
| AE1/3 | Agilent, M351501-2 | 1:100 | Epithelial cells | |

*associated Opal fluorophores are shown in brackets, all from Akoya Biosciences



AJRCCM Articles in Press. Published November 20, 2020 as 10.1164/rccm.202008-3265OC

## References


1. Osborn ML, S.; Stewart, R.; Swift, B.; Youd, E. Autopsy practice relating to possible cases of COVID-19 (2019-nCov, novel coronavirus from China 2019/2020). The Royal College of Pathologists; 2020.
2. Hsia CCW, Hyde DM, Ochs M, Weibel ER. An Official Research Policy Statement of the American Thoracic Society/European Respiratory Society: Standards for Quantitative Assessment of Lung Structure. Am J Respir Crit Care Med 2010;181:394-418.
3. nCoV-2019 sequencing protocol. 2020. (Accessed 1/6/2020, 2020, at https://www.protocols.io/view/ncov-2019-sequencing-protocol-bbmuik6w.)
4. Bankhead P, Loughrey MB, Fernandez JA, et al. QuPath: Open Source Software for Digital Pathology Image Analysis. Sci Rep 2017;7:16878.
5. Shi H, Han X, Jiang N, et al. Radiological findings from 81 patients with COVID-19 pneumonia in Wuhan, China: a descriptive study. Lancet Infect Dis 2020;20:425-34.
6. Ranieri VM, Rubenfeld GD, Thompson BT, et al. Acute respiratory distress syndrome: the Berlin Definition. JAMA 2012;307:2526-33.
7. Docherty AB, Harrison EM, Green CA, et al. Features of 20 133 UK patients in hospital with covid-19 using the ISARIC WHO Clinical Characterisation Protocol: prospective observational cohort study. BMJ 2020;369:m1985.




AJRCCM Articles in Press. Published November 20, 2020 as 10.1164/rccm.202008-3265OC